geosciences

MDPI

Article

A Multi-Method Approach for Deciphering Rockshelter Microstratigraphies—The Role of the Sodicho Rockshelter (SW Ethiopia) as a Geoarchaeological Archive

Elena A. Hensel [1,*], Martin Kehl [1], Luisa Wöstehoff [2], Katharina Neumann [3], Ralf Vogelsang [4] and Olaf Bubenzer [5]

1 Institute of Geography, University of Cologne, 50923 Cologne, Germany; kehlm@uni-koeln.de
2 Institute of Crop Science and Resource Conservation—Soil Science and Soil Ecology, University of Bonn, 53113 Bonn, Germany; luisa.woestehoff@gmail.com
3 Institute of Archaeological Sciences, Senckenberg Research Institute, Goethe University, 60323 Frankfurt am Main, Germany; k.neumann@em.uni-frankfurt.de
4 Institute of Prehistoric Archaeology, University of Cologne, 50931 Cologne, Germany; r.vogelsang@uni-koeln.de
5 Heidelberg Center for the Environment (HCE), Institute of Geography, Heidelberg University, 69120 Heidelberg, Germany; olaf.bubenzer@uni-heidelberg.de
* Correspondence: elena.hensel@uni-koeln.de; Tel.: +49-(0)-221-470-6524

Abstract: The Sodicho Rockshelter in the southwestern Ethiopian Highlands presents a unique site that contains sediments of Upper Pleistocene and Holocene occupation phases of hunter-gatherer communities. Excavations and previous geoarchaeological research provided a first ^{14}C chronostratigraphic framework for the last 27 ka cal BP, which supports the hypothesis of a potential environmental refugium during the Late Glacial Maximum (LGM, ~21 ± 2 ka). Nonetheless, it is necessary to extend the preliminary interpretation of stone tool assemblages, and the geoarchaeological analyses carried out so far to provide in-depth information on prehistoric human behavior at the site under changing climatic and environmental conditions. In this study, we reinvestigate the complex stratigraphy and the paleoclimatic context of Sodicho in order to expand the knowledge about site formation, post-depositional disturbances, weathering influences, and the anthropogenic impact on the sediment deposits. Micromorphological observations and the determination of active pedogenic oxides offered a more detailed look at the microstratigraphic record in relation to shifting moisture conditions during the African Humid Period (AHP, ~15 − 5 ka). Sediment alteration and reworking are connected to the influence of sheet flow, biological activity, and human impacts such as dumping activity and site maintenance. A comparison with black carbon (BC) analyses and a qualitative phytolith ratio (quantification of dark and light phytoliths) provided evidence for variations in human fire intensity. Our collaborative and multidisciplinary approach demonstrates how the complex formation of a rockshelter site in a tropical setting with changing climatic and anthropogenic impacts can be tackled.

Keywords: geoarchaeology; Ethiopia; rockshelter; Upper Pleistocene; Holocene; micromorphology; black carbon; phytoliths; pedogenic oxides

check for updates

Citation: Hensel, E.A.; Kehl, M.; Wöstehoff, L.; Neumann, K.; Vogelsang, R.; Bubenzer, O. A Multi-Method Approach for Deciphering Rockshelter Microstratigraphies—The Role of the Sodicho Rockshelter (SW Ethiopia) as a Geoarchaeological Archive. *Geosciences* **2022**, *12*, 92. https://doi.org/10.3390/geosciences12020092

Academic Editors: Rossana Sanfilippo and Jesus Martinez-Frias

Received: 14 December 2021
Accepted: 8 February 2022
Published: 17 February 2022

Publisher's Note: MDPI stays neutral with regard to jurisdictional claims in published maps and institutional affiliations.

Copyright: © 2022 by the authors. Licensee MDPI, Basel, Switzerland. This article is an open access article distributed under the terms and conditions of the Creative Commons Attribution (CC BY) license (https://creativecommons.org/licenses/by/4.0/).

1. Introduction

The sediment deposits at the Sodicho Rockshelter, a volcanic rockshelter in the southwestern Ethiopian Highlands, provide important evidence for hunter–gatherer occupation over the last 27 ka years, thereby partly closing one of the major chronological gaps associated with the time range of Marine Isotope Stage 2 (MIS 2) [1]. Located near the Mochena Borago Rockshelter, a key site documenting Upper Pleistocene hunter–gatherer communities [2–4], Sodicho offers a complementary stratigraphy. Since the bedrock has not yet been reached during the excavations, further deposits are expected at Sodicho.

The stratigraphy of an archaeological site, ideally in an intact and undisturbed state, illustrates the occupational history and behavior of past inhabitants, as well as past environmental conditions. Often, rockshelters provide excellent sediment traps. Nevertheless, stratigraphies can be influenced by changing depositional environments and post-depositional impacts [5]. Particularly, this holds true for stratigraphies of rockshelters in tropical regions, which are often subject to changing moisture conditions [5,6]. This can complicate the identification of sedimentary sources and depositional processes at these sites.

Geoarchaeological methods, such as sediment analyses, micromorphology, or geochemical investigations, allow the study of various depositional processes and add a geomorphological and geoscientific perspective to archaeological investigations. In particular, micromorphological observations allow conclusions about sediment alteration, translocation processes, and human activity at a site [7].

Prior geoarchaeological research at Sodicho revealed a complex depositional history, influenced by depositional circumstances of the Late Glacial Maximum (LGM, ~21 $\pm$ 2 ka) and the Early Holocene African Humid Period (AHP, ~15 $-$ 5 ka BP) [1,8,9]. Past humans used the rockshelter repeatedly, probably during both dryer and wetter phases. However, an in-depth microscopic analysis of the deposits that would offer a better understanding of the stratigraphy and possible human–environment interactions had not been carried out yet. Therefore, we conducted a multi-method approach to specify human behavior, such as the use of fire. First, we employed micromorphological thin section analysis to determine the composition and the spatial structure of identified features that are not visible to the naked eye [7,10]. Especially regarding site formation processes and activity of prehistoric humans in caves and rockshelters, micromorphological studies have proven to be an essential tool. Among many in-depth studies, the interplay of geogenic, biogenic, and anthropogenic processes were studied at several sites, for instance, in southern [11–13] and northern Africa [14–16], the Levant [17,18], the Iberian Peninsula [19], central Europe [20], Western Australia [21], central Asia [22], and southern Siberia [23,24]. These studies emphasized the significance of humans as depositional agents and allowed a better understanding, in particular about palaeoenvironmental changes, human activity zones, combustion practice, combustion bi-products, and synsedimentary human activity, such as trampling and site maintenance.

In this study, black carbon (BC) measurements are used as a proxy for fire residue input and past human–fire interactions. The term BC describes the sum of pyrogenic organic matter and may comprise all charred residues, charcoal, and soot particles [25]. The aromatic structures [26,27] render BC recalcitrant to decomposition so that it can remain in soil and sediments for several thousands of years (e.g., [28–30]). To quantify the total amount of BC and also its properties (the latter to indicate changes in fire temperature), we determined benzene polycarboxylic acids (BPCAs) as specific tracers [31–33].

Further verification of fire residue input provides a preliminary qualitative phytolith analysis in order to develop a simple ratio of burned and unburned phytoliths. Opal phytoliths, as inorganic silicate bodies, are produced in plant cells or the cell wall through polymerization of monosilicic acid (H_4SiO_4) taken up by plant roots [34–36]. Dark discoloration of the phytoliths is often caused by exposure to a fire, which burns occluded natural carbon or plant organic tissue, suggesting either natural bushfire or human-induced fire activity [10,34,35,37].

Finally, we determined the concentration of active iron (Fe), silicon (Si), aluminum (Al), and manganese (Mn) in an acidified ammonium oxalate (AO) extract [38,39]. In soil science, the AO method has been regarded as quantifying poorly crystalline or amorphous pedogenic (hydr)oxides formed after deliberation of the metals by silicate weathering. However, other species, such as organic associations or poorly crystalline aluminosilicates, may be dissolved by the AO extract as well [40].

The main aims of this study are (a) the extension of knowledge about the site formation processes and post-depositional alteration of the stratigraphy during the last 27 ka years,

(b) the identification of microscopic evidence on the degree of weathering under the influence of changing humidity within the rockshelter, (c) the determination of human activities with emphasis on the reconstruction of human fire activity, and finally (d) to demonstrate that such a geoarchaeological multi-method approach allows tackling complex rockshelter stratigraphies in a tropical environment in general.

2. The Site: Setting and Background

Sodicho Rockshelter is a ~30 m deep cavity on the southern flank of the trachytic Mount Sodicho, a volcanic mountain in the southwest Ethiopian Highlands (E 37°36′44 and N 7°15′21). The research area lies west of the southern Main Ethiopian Rift and the southern Ethiopian Plateau, east of the Omo River Canyon, and south of the three circular Wagebeta Calderas (Figure 1a). It is characterized by past volcanic activity and tectonic stress that occurred during the late development of the Ethiopian rift system [41–44]. The natural vegetation of Mount Sodicho is subject to drastic changes as a result of recent human impact. Nowadays, dense settlement, agriculture and cattle farming, human-induced deforestation, and massive soil erosion are characteristic, in particular at the relatively flat summit and the slopes. The average precipitation is 2000 mm per year. Still, annual and inter-annual precipitation changes have an effect on the vegetation cover (Figure 1b,c).

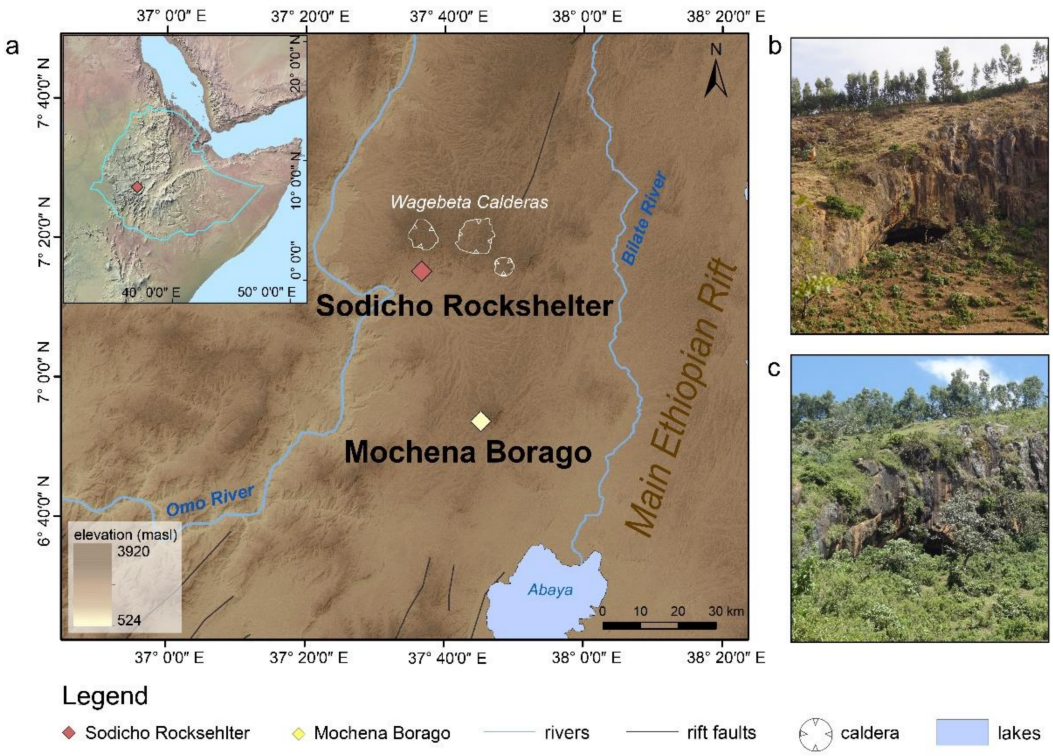

Figure 1. (**a**) Map of the study area in the Southwestern Ethiopian Highlands (DEM data by ASTER GDEM and Natural Earth raster map data); (**b**) During the dry season, natural plant growth is significantly reduced (photo by R. Vogelsang, 16 February 2016); (**c**) Mount Sodicho is heavily vegetated after the main rainy season (photo by E. Hensel, 18 November 2018).

The mountain itself has an irregular dome structure affected by an episodic and permanent hydrological system [44]. River erosion and gully formation are common phenomena, leading to the exposure of scattered obsidian raw material. Recent soil erosion exposed relatively fertile, red-colored, and kaolinite-rich humic Nitisols, typical for the tropical highlands [45,46].

The south-facing opening of the rockshelter is located below steep rock walls. Large boulders (3–4 m) prevent direct access to the cave and thus the direct influence of weather

conditions. The trachytic bedrock is grey to yellowish in color and erodes easily in certain places. During and immediately after the rainy season, the shelter is affected by the water dripping down the ceiling, resulting in constant dripping areas, the formation of shallow pools and drip holes, as well as weathering of large boulders within the cave. The rock surface of the walls is affected by dark staining, alveolar weathering (honeycomb weathering), and uneven exfoliation. During dry periods, evidence of residual moisture is limited to damp areas in the rear of the rockshelter.

The Sodicho Rockshelter, first visited by our team during surveys in 2012, lies ~40 km away from the key site Mochena Borago Rockshelter located on the southwestern slope of Mt. Damota. Mochena Borago has been well investigated since 1998 and contains Upper Pleistocene sedimentary units and cultural remains dated to >50 ka to ~36 ka and the Holocene [2,3,47,48]. The excavations at Sodicho were undertaken annually from 2015 to 2018 in the backward area of the rockshelter, starting with two test pits of 50 × 50 cm (Figure 2). The main pit was extended to 4 m^2 down with a maximum depth of ~2 m without reaching the bedrock. In 2016, a third pit (50 × 50 cm) with a depth of 60 cm was added [1].

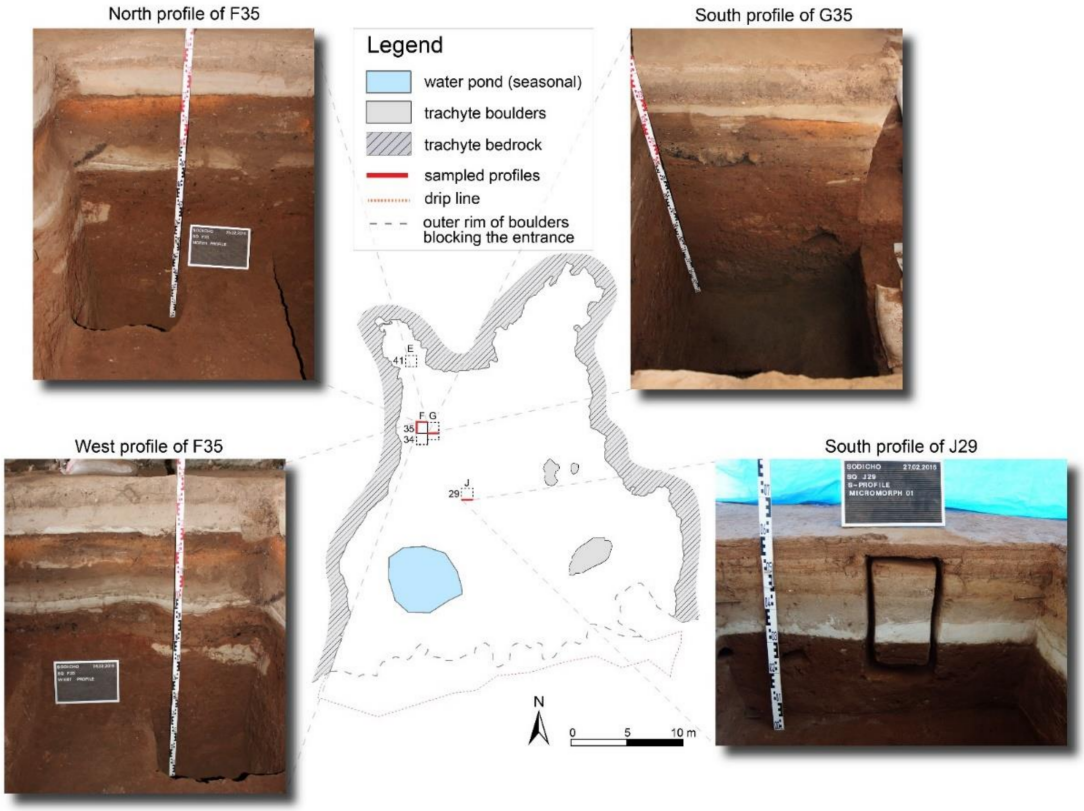

Figure 2. Floorplan of the Sodicho Rockshelter showing images of the excavation pits mentioned in the text (photos by R. Vogelsang, February 2016).

The most recent geoarchaeological investigations at Sodicho Rockshelter comprise a selection of sedimentological and geochemical analyses and the establishment of a chronological framework with ^{14}C dating. So far, a complex stratigraphy with nine sediment units was identified that include five anthropogenic units (in terms of geogenic sediment deposits impacted by human activity during occupation phases I, III, V, VII, and IX), three distinct allochthonous tephra units (II, IV, VIII) and a thick clayey archaeologically sterile unit (VI) (Figure 3) [1].

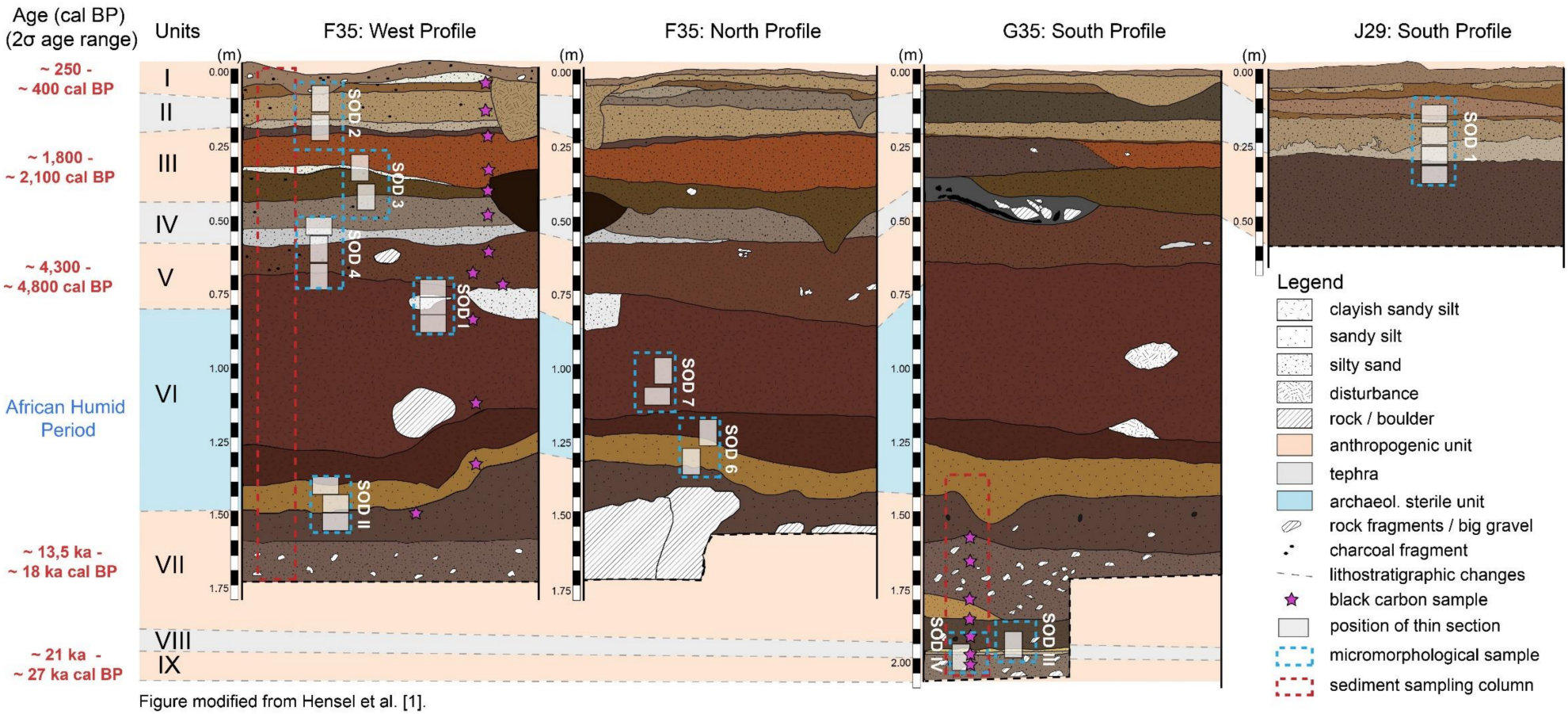

Figure 3. Schematic illustration of the excavation profiles F35 west and north, G35 south and J29 south. Red ages refer to calibrated ^{14}C age range of 31 radiocarbon samples. Sediment samples are indicated in red, micromorphological sample blocks in blue, thin sections as whitish squares and BC samples as stars. A rockfall layer is in the upper part of Unit VII is illustrated in square F35 as white crosshatched boulders. The relative thicknesses of the sediment units are indicated in the background by different colors (mod. [1]).

According to macroscopic observations in the field, the deposits are slightly tilted to the northern backwall of the shelter. The occupational layers are recognized by a mostly dark brownish sediment color with an average grain size of silt and fine sand. In addition, some layers of these units show sediment rubification. Cultural remains and structures include lithic obsidian artifacts, macroscopic charcoal, hearths, and pits. Bone material has not been preserved in layers older than some hundred years due to the moist and acidic milieus of the sediments. The cultural units have a certain sedimentological fingerprint, characterized by higher values of total organic carbon (TOC), magnetic susceptibility (MS), manganese (Mn), and phosphorus (P) (Figure 4) [1]. The presence of hearth features and the lateral distribution of macroscopic evidence for fire residue in Unit III and V [1] represent in situ burning events as known from other rockshelter sites [49].

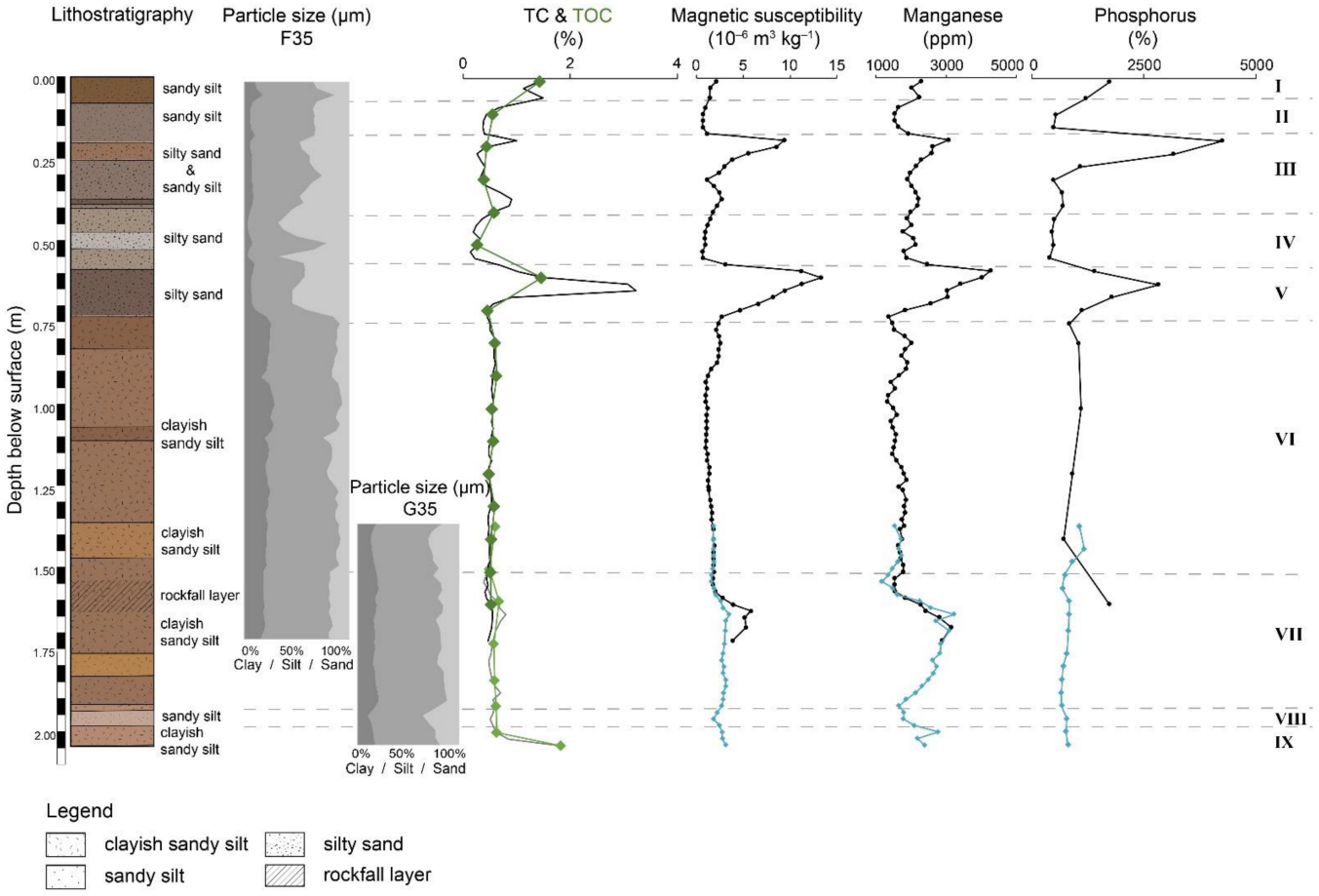

Figure 4. Sedimentological and geochemical properties of the profile F35 (black graphs) and G35 (grey graphs): carbon content with TC and TOC (green graph); magnetic susceptibility, element trends (manganese and phosphorus) (mod. [1]).

Radiocarbon measurements, mainly of charcoal, date the upper anthropogenic units between ~1800 and ~2100 cal BP (Unit III) and ~4300 and ~4800 cal BP (Unit V) [1]. Both units contain obsidian microlithic stone tools such as backed microliths, characteristic of the African Later Stone Age (LSA). Pottery and bone are also present but are limited to the youngest Later Stone Age assemblage (Unit III) and the surface layer (Unit I). Stratigraphically lower settlement layers date between ~13,500 and ~27,000 cal BP (Unit VII and IX) and contain predominantly obsidian artifacts. A rockfall layer with trachytic boulders (max. 70 cm in diameter) is located in the upper part of Unit VII. The boulders are weathered with a rounded upward-facing surface, indicating a slow covering with sediment. Allochthonous geogenic deposits (tephra layers, Unit II, IV, VII) are recognizable

by their light coloration and coarser grain size from fine sand to coarse sand [1]. Tephra units are mostly multi-layered, with a slightly darker upper layer often containing brown angular lenses. In Units II and IV, transitional layers are found underneath, which contain fine graduation/lamination visible to the naked eye. The mentioned archaeologically sterile Unit VI is a ~60 cm thick deposit of autochthonous and allochthonous geogenic sediment that can be dated to the African Humid Period. It is characterized by increased clay content and a continuous reddish-brown coloration. Increased values of Fe_2O_3, aluminum (Al), and titanium (Ti), and a lower K/Rb ratio point to intense weathering of this unit [1].

3. Material

The material for this study was sampled during the annual excavations in 2016 to 2018. In the following, the individual sampling strategy and the position within the stratigraphy are described. A detailed description of the methodology can be found in Appendix A.

A sampling of undisturbed sediment blocks for the micromorphological investigation was conducted at four excavation profiles (F35 North, F35 West, G35 South, J29 South) (Figure 3). Thin sections of samples taken in 2016 are labeled with Arabic numerals and those taken in 2018 with Roman numerals. The samples were taken from sediment units and across layer boundaries to ensure a sampling of the variety of depositional processes and to detect (environmental) transition zones. A large boulder, which only became visible when attempting to remove the sample block SOD_III, considerably complicated the sampling. The lower part of this sample might be disturbed, which was considered in the following interpretations. The thin sections are classified into predominant facies types according to the stratigraphic description of Sodicho by Hensel et al. [1] and the defined deposition units. In this process, we distinguish individual micromorphological subunits by color, composition, compaction, and changes in grain size fractions.

A total of 20 sediment samples were taken from two excavation squares F35 and G35 (Table A1), for the analysis of black carbon (BC) covering anthropogenic deposits, light-colored tephra, and the archaeologically sterile section. For the phytolith study, ca. 10 g of thirteen bulk sediment samples were collected from excavation squares F35, and seven samples were taken from G35. To determine AO extractable Fe, Si, Al, and Mn, 20 reference bulk sediment samples were selected from the stratigraphy.

4. Results

4.1. Micromorphology

The most important features of each unit are described in stratigraphic order beginning with the lowest unit IX. Detailed results of the thin section analyses are presented in Table S1. The defined stratigraphic units within each thin section were divided into subunits, according to macroscopic boundaries detected in the flat bed scans (Figure 5).

Overall, the micromorphological observation verified the diverse stratigraphy with repetitive occupation layers, alternating with volcanic ash (tephra) or non-anthropogenic clayey layer. Independent of the sedimentological units, the following features can be identified in the majority of the thin sections. According to the micromorphological investigations, major coarse components (>10 µm in diameter) in the cultural layer (Units I, III, V, VII, and IX) and the archaeologically sterile unit VI are trachytic rock fragments of the bedrock of the shelter, feldspar mineral grains, brown clay and silt granules, and varying amounts of opal phytoliths with a whitish to bluish-white interference color under oblique incident light (OIL). Volcanic glass is the predominant coarse material within the tephra in Units II, IV, and VIII and within weathered tephra in Unit VI. Beyond that, volcanic glass particles are also mixed into the matrix within the other stratigraphic units but in different states of weathering. Anthropogenic coarse features are fragments of obsidian, bone, and charcoal. The following descriptions of the micromorphological results are presented from the bottom (Unit IX) to top (Unit I):

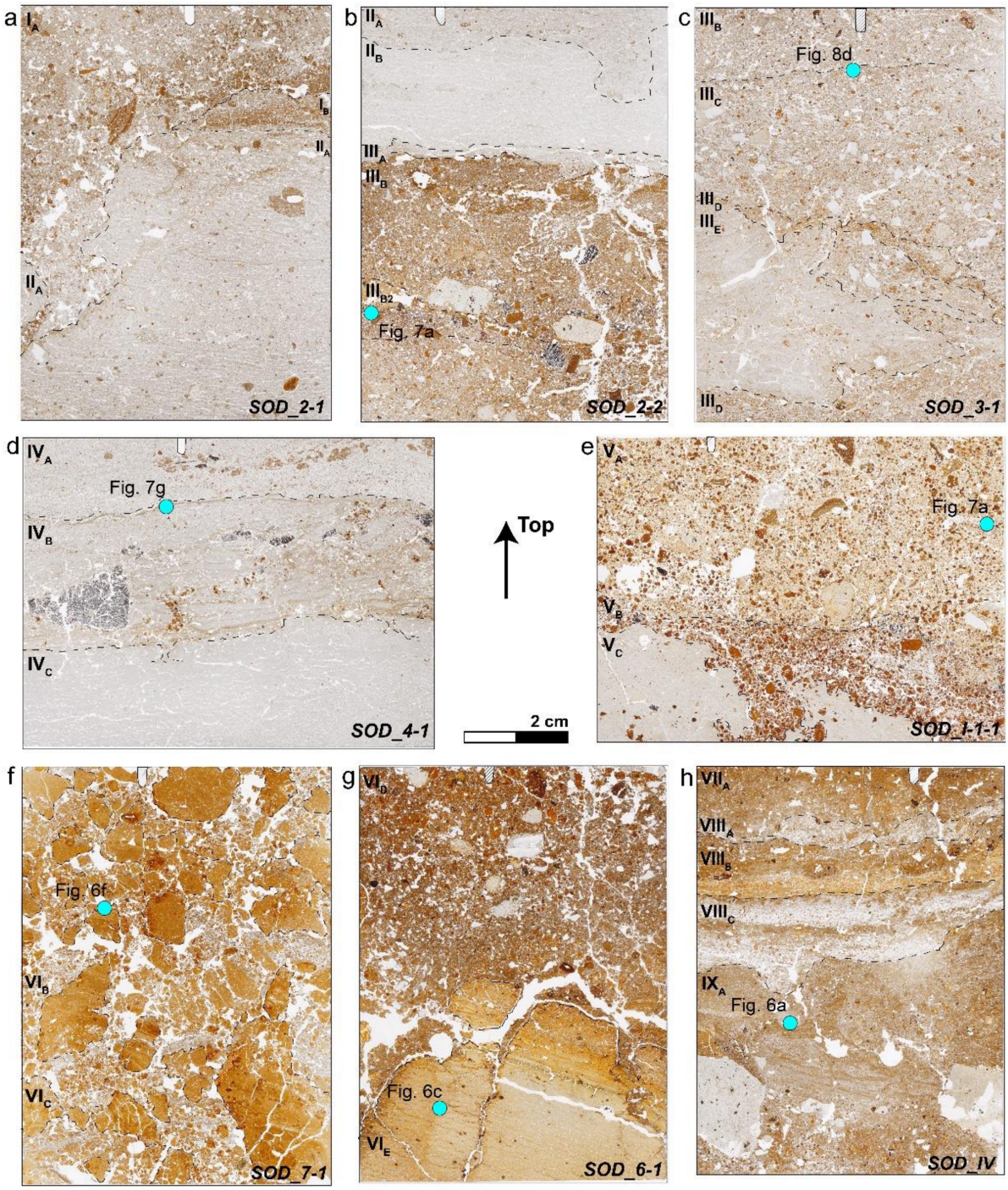

Figure 5. Flatbed scans of representative thin sections from Sodicho Rockshelter captured in transmitted light mode; subunits are indicated with Roman numerals and letters in subscript; green dots refer to figures mentioned in the text. (**a**) Transition between Unit II and I in SOD_2-1. (**b**) Sharp boundary between anthropogenic Unit III and tephra (Unit II) in SOD_2-2. (**c**) Disturbed tephra within the anthropogenic Unit III in SOD_3-1. (**d**) Multi-layered tephra (Unit IV) in SOD_4-1. (**e**) Fragments of charcoal and burned bone above a disturbed tephra in SOD_I-1-1 (Unit V). (**f**) Fragmented and deformed sediment aggregates in a finer matrix in SOD_7-1 (Unit VI). (**g**) Yellow, weathered tephra in the lower part of SOD_6-1 (Unit VI). (**h**) Multi-layered and disturbed tephra (Unit VIII) in the lowermost micromorphological sample SOD_IV.

4.1.1. Unit IX

The anthropogenic Unit IX is represented in the lower parts of the thin sections SOD_IV and SOD_III (Figure 5h). Microscopically, the deposits show a vughy microstructure. Coarse features consist mainly of individual feldspar mineral grains, fragmented charcoal particles, trachytic rock fragments with a fluidal feldspar texture, and bigger feldspar phenocrysts. Fine layered aggregates of volcanic glass particles and aggregates with phytoliths, as well as fragmented aggregates with finely graded bedding, are included. A large number of well-preserved light and a few dark phytoliths are found in a 0.5 cm depression-shaped accumulation, which also contains brown clay aggregates in the same fine particle size (Figure 8a). Main pedofeatures are fragments of bright yellow-orange colored clay coatings and limited bioturbation, indicated by biogenic pores. All included components and aggregates are intermixed within a brownish, dotted, and speckled micromass. The boundary to the overlying subunit VIII_C is sharp.

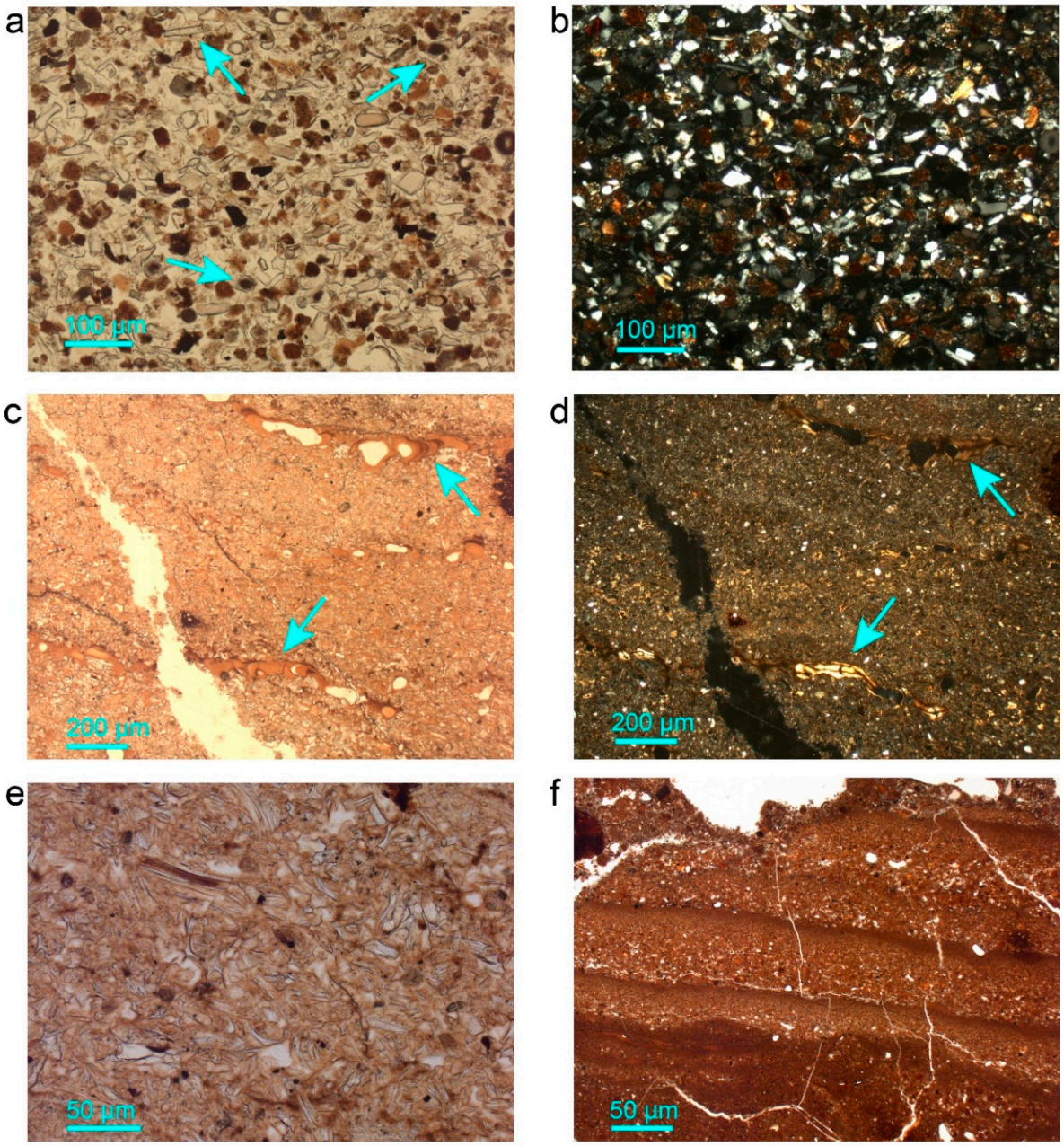

Figure 6. *Cont.*

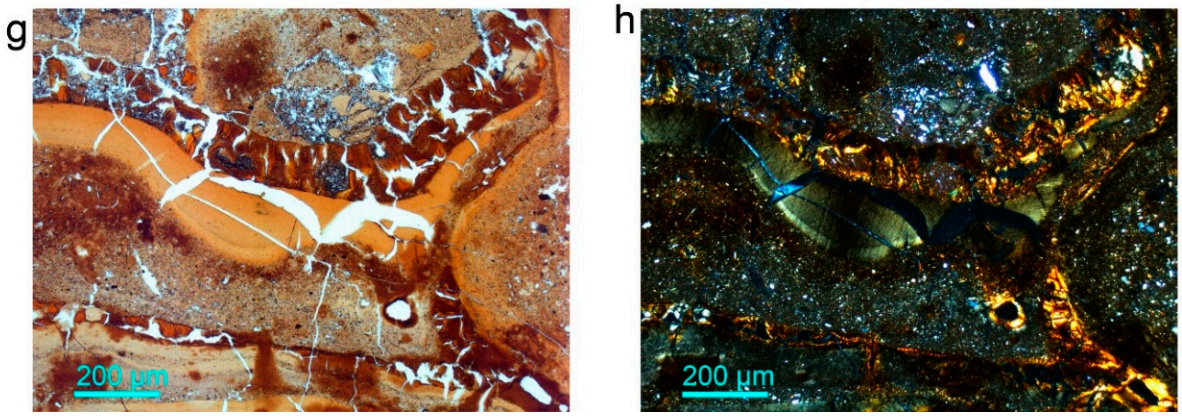

Figure 6. Microscopic images of thin sections from the Sodicho Rockshelter. (**a**) Aggregation of light phytoliths (green arrows), brownish clay aggregates and rounded feldspar particles within subunit IX_A (SOD_IV, PPL). (**b**) Optically isotropic phytoliths remain black under XPL, same as Figure 8a (XPL). (**c**) Highly weathered tephra with an abundance of yellowish clay (green arrows) (SOD_6-1, PPL). (**d**) Limpid clay coatings with yellowish golden color, same as Figure 8c (XPL). (**e**) Weathering of the volcanic glass particles in a yellow clayey micromass (SOD_6-1, PPL). (**f**) Graded silt and clay bedding in an aggregate (SOD_7-1, PPL). (**g**) Reddish crystalized Fe-(hydr)oxides coatings on top of yellow clay coating along voids (SOD_7-2, PPL). (**h**) Differences in birefringence colors are obvious, same as Figure 8g (XPL).

4.1.2. Unit VIII

The geogenic Unit VIII, approximately three cm thick, has a complex structure with a sequence of three thin subunits, which are preserved in thin section SOD_III and particularly well in SOD_IV. In these subunits, the coarse components consist of volcanic glass particles in different states of weathering. The lowest subunit (VIII_C) appears very loose with large porosity and includes two white tephra layers with intermixed brownish-grey sediment. The layers are separated by a brownish silty layer containing only a few sharp-edged volcanic glass particles. The upper part of this subunit ends with a compacted crust of light pale clay, followed by a subunit (VIII_B) of yellowish tephra. The lower part consists almost entirely of weathered volcanic glass and yellowish clay coatings (textural pedofeature) (Figure 5h). The micromass of this subunit has a speckled limpidity and grano-, porostriated b-fabric. The uppermost subunit VIII_A is characterized by volcanic glass particles mixed in a brownish-grey matrix. The most prominent pedofeatures of this unit are yellowish clay coatings with bright interference colors.

4.1.3. Unit VII

The sediment of anthropogenic Unit VII seems relatively uniform and cannot be subdivided, according to the micromorphological observations. As the sediment of this unit and the features contained within the thin sections are similar, only one subunit is described. The unit is visible in thin sections SOD_6-2, SOD_II_3-3, SOD_III, and SOD_IV. Coarse components consist of slightly rounded trachytic rock fragments, charcoal fragments, and rounded granules in a reddish-brown clayey silt matrix. Fine volcanic glass with rounded edges and phytoliths are common within the brownish dotted micromass. Biogenic pedofeatures consist of passage features and biogenic pores. Further pedofeatures include redoximorphic nodules, yellow limpid clay coatings, and clay papules (fragmented clay coatings). In addition, sporadic lenses of fine, compacted sediment (disturbed crust material) are common.

4.1.4. Unit VI

The archaeologically sterile Unit VI can be divided into five subunits based on the micromorphological observations within the thin sections SOD_I_1-2, SOD_I_1-3, SOD_I_4-

1, SOD_7-1, SOD_7-2, SOD_6-1, SOD_6-2, SOD_II_3-1, and SOD_II_3-2. In the field, the color of the dark reddish-brown sediment appeared homogenous, but differences in composition and layering of Unit VI are evident on a microscopic scale. The only apparent subdivision is a yellowish tephra layer (VI_E and VI_{E2}) in the lower area (Figure 5g), which is the sharp boundary to the underlying Unit VII. Several accommodating aggregates (10 to 20 cm thick) of yellow and heavily weathered tephra form the subunit VI_E. The aggregates have a vuhgy microstructure with a very high proportion of limpid clay coatings with a bright interference color and a grano- and porostriated b-fabric of the clayey micromass. Vesicle chambers and channels are aligned parallel to each other. Furthermore, there are a few coatings with undifferentiated limpidity. The volcanic glass, as the main component, is extremely weathered, with round edges and particle fragmentation. There are sections with finely graded bedding of volcanic glass of silty grain size.

The weathered tephra is followed by reddish-brown silty clay sediment (Unit VI_D) with a dotted and speckled micromass and a stipple-speckled and partly undifferentiated b-fabric. In the thin sections SOD_6-1, SOD_II-3-1, and SOD_II_3-2, the porosity is low. The proportion of coarse feldspar mineral grains is increased in SOD_6-1, SOD_6-2, and SOD_II_3-1. The subunit VI_C consists mainly of clayey-silty sediment, broken into yellow-reddish and brownish, rounded to subangular aggregates with a vughy microstructure. Several bigger (up to 2 cm diameter) aggregates are internally fragmented (accommodated to partly accommodated). The clayey to silty aggregates are very diverse in texture, especially within the thin sections SOD_7-1 and SOD_7-2. Some aggregates include well-developed rhythmic bedding of fine silt and clay as well as microlaminated illuvial clay coatings. In certain areas, the clay coatings are impure with a speckled limpidity. Redoximorphic features are observed as dark reddish-brown Fe/Mn oxide nodules, along with a mainly reddish-brown coloring of the groundmass. The aggregates increase in size towards the top and can reach sizes >1 cm.

The sediment between the aggregates (VI_B) in SOD_7-1 and SOD_7-2 appears more dispersed with higher porosity. Coarse components include trachyte fragments of the bedrock, feldspar mineral grains, and rare charcoal fragments in the upper part. There are also differences in the fine sediment between the aggregates. The main components are silty brown granules and an equal proportion of transparent volcanic glass, which are intermixed and fragmented. Furthermore, reddish needle-shaped coatings and a fanlike intergrowth are present in the samples SOD_7-1, SOD_7-2, and SOD_I-1-3 (Figure 8g). The most prominent impregnative pedofeatures are Fe/Mn hypocoatings and redoximorphic nodules, which are particularly pronounced within the uppermost subunit VI_A. Biogenic pores are found in all subunits of Unit VI and especially pronounced in the samples SOD_II-3-1 and SOD_7-1.

4.1.5. Unit V

The anthropogenic Unit V can be divided into four subunits, which can be observed in thin sections SOD_4-2, SOD_4-3, SOD_I-1-1, SOD_I-1-2, and SOD_I-4-1. The whole unit is affected by post-depositional disturbance indicated by passage features, reworked sediment, and lateral translocation of coarse components, e.g., charcoal and bone fragments. There is no horizontal orientation of elongated components. The lower subunit V_D occurs in SOD_I-1-2 and SOD_I-4-1 from the west profile F35 and consists of reddish-brown silt and clay sediment. Some granules (angular blocky microstructure) show fine graded bedding and lamination, resembling the sediment of Unit VI.

The micromorphological sample SOD_I is unique as it contains fire residues such as charcoal and rubified sediment (V_B), overlying a redeposited light-colored tephra (V_C) (Figure 7a,b). In addition, colorless calcined bone fragments are observed in PPL, which appear with dull interference colors under XPL. Within subunit V_B, calcitic ash was not found, and burned materials were mixed with unburned. The term redeposited is used because the tephra is not a continuous layer in the stratigraphy but rather lies in a kind

of depression. An accumulation of feldspar mineral grains with pellicular alteration (Figure 7c,d) is found below the tephra (V_D).

The uppermost subunit V_A has a vughy microstructure and is characterized by a mainly pale yellowish isotropic groundmass (Figure 5e) with a dotted limpidity and an undifferentiated b-fabric. Coarser components in this subunit are trachytic rock, feldspar mineral grains, obsidian artifacts, charcoal fragments, calcined bone fragments, and rounded silty clay granules. Biogenic silicate is also found in the form of dark phytoliths and clustered SPHEROID ORNATE phytoliths (Figure 8a). In addition, volcanic tephra lenses (V_{A2}) are observed in this subunit V_A, showing graded bedding of rounded volcanic glass particles. Pedofeatures comprise passage features, limpid clay coatings, and brownish silt-clay coatings around bigger trachytic fragments.

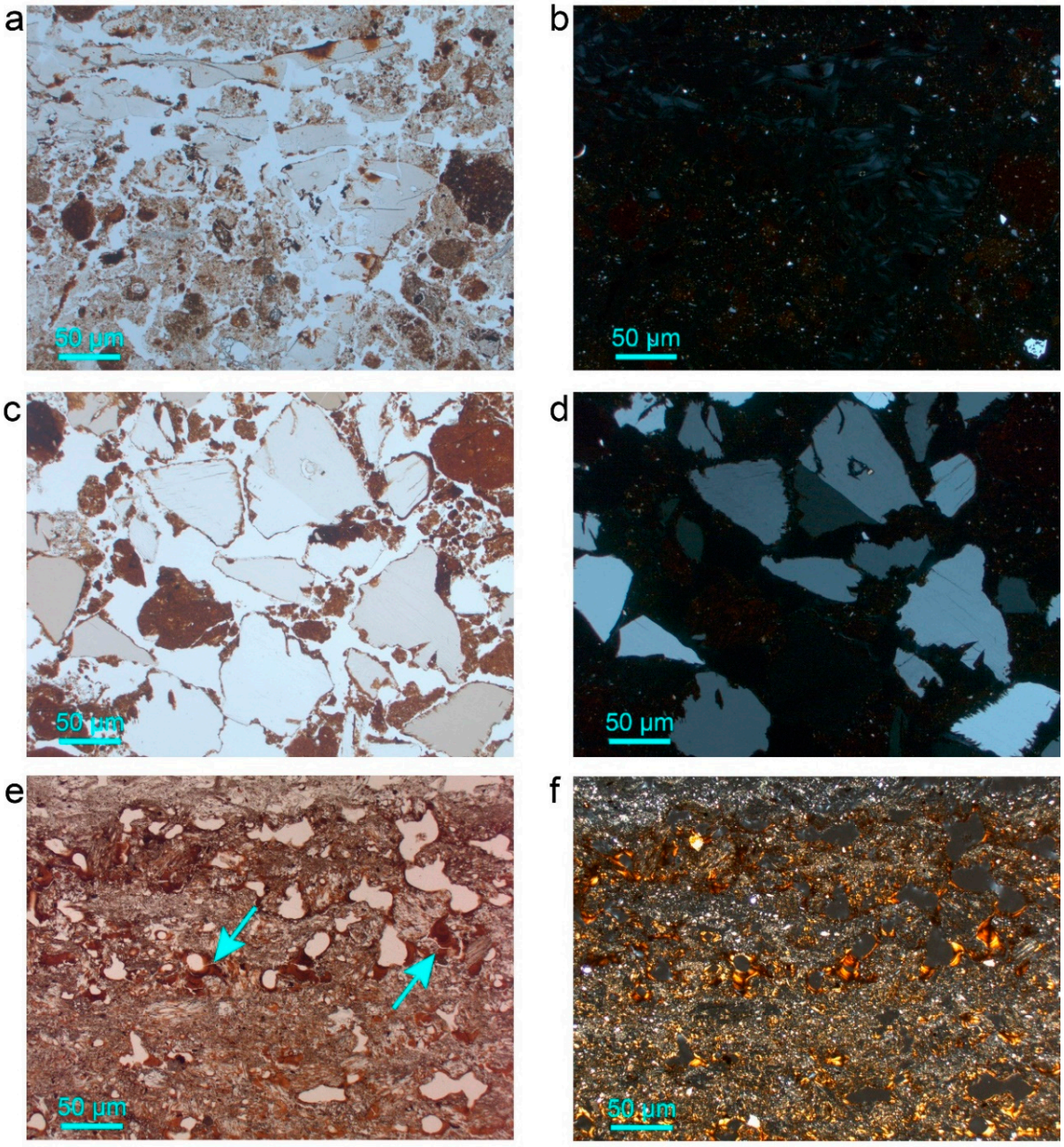

Figure 7. *Cont.*

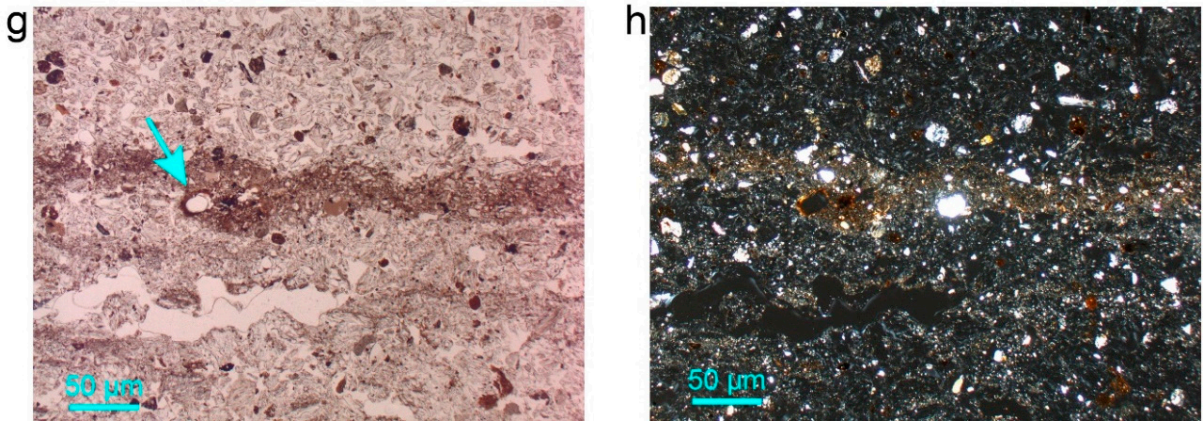

Figure 7. Microscopic images of thin sections from the Sodicho Rockshelter. (**a**) Fragmented and calcinated bone within fire residue (SOD_I-1-1, PPL). (**b**) Bone fragments show very weak interference colors, same as Figure 7a (XPL). (**c**) Accumulation of altered feldspar mineral grains (SOD_I-4-1, PPL). (**d**) Same as Figure 7c (XPL). (**e**) Weathered volcanic glass and reddish-brown clay coatings (green arrows) (SOD_4-2, PPL) (**f**) Clay coatings with reddish-golden interference colors, same as Figure 7e (XPL). (**g**) Fine brownish banding within tephra and brownish clay coatings (green arrow) (SOD_4-1, PPL). (**h**) Same as Figure 7g (XPL).

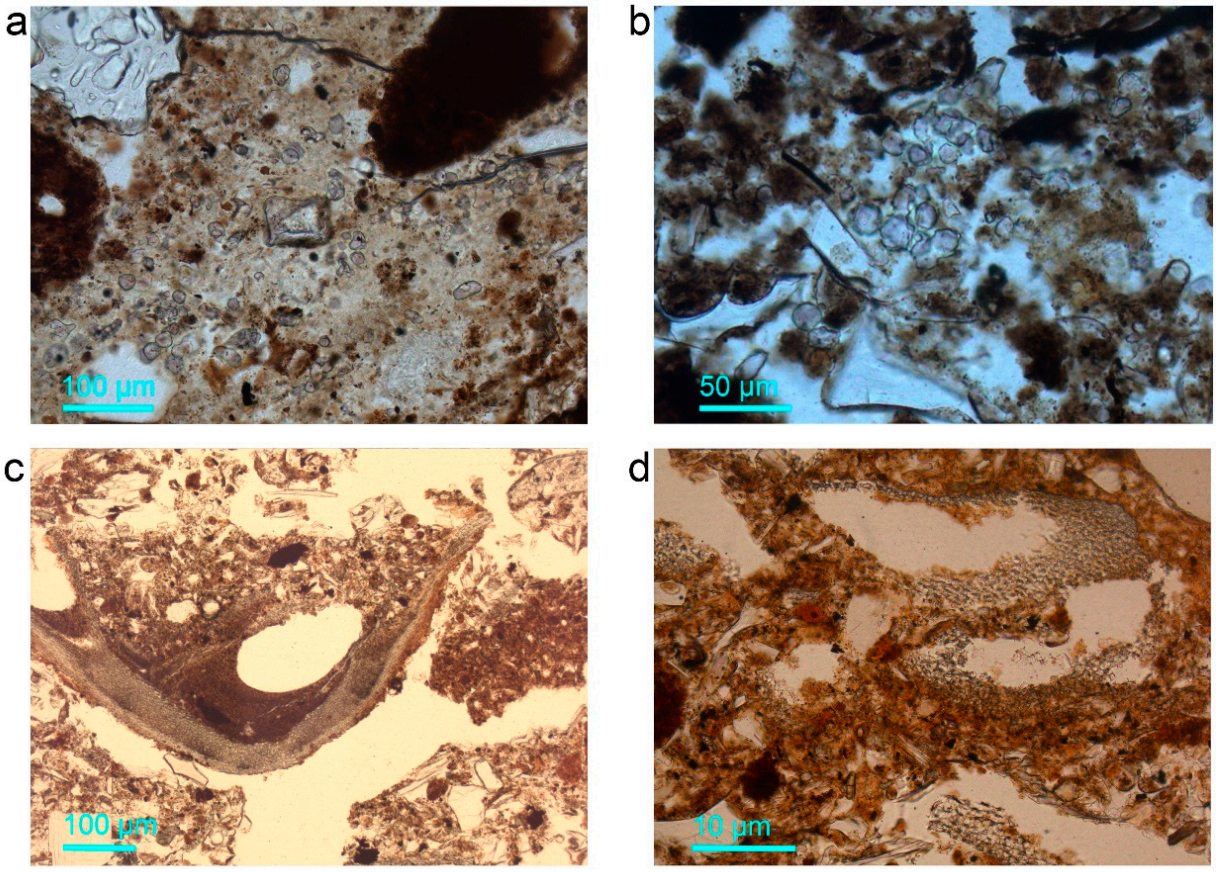

Figure 8. *Cont.*

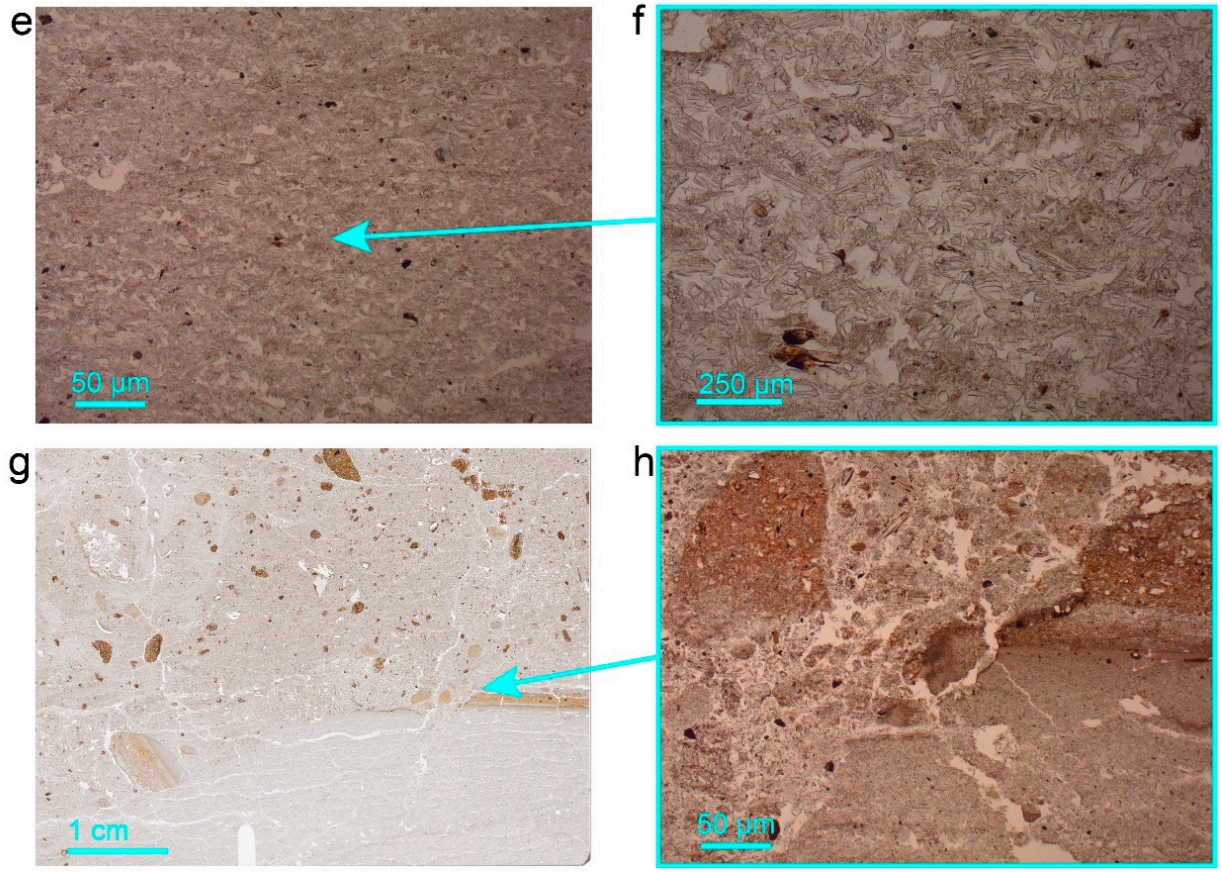

Figure 8. Microscopic images of thin sections from the Sodicho Rockshelter. (**a**) Spherical phytoliths within yellowish sediment of Unit V (SOD_I_1-1, PPL). (**b**) Magnification of spherical phytoliths within organic-rich sediment of Unit III (SOD_2-2, PPL). (**c**) Fragment of undefined fruit seed coats/shells (SOD_3-1, PPL). (**d**) Magnification of fine seed coat fragments (SOD_3-1, PPL). (**e**) Light tephra with brownish sediment particles (SOD_1-3, PPL). (**f**) Magnification of the same section (SOD_1-3, PPL). (**g**) Two tephra layers are separated by a yellow clay crust (SOD_1-2, PPL). (**h**) Magnification of the clay crust and an erosional contact (SOD_1-2, PPL).

4.1.6. Unit IV

The geogenic Unit IV, visible in thin sections SOD_3-1, SOD_4-1, and SOD_4-2, can be divided into four subunits. The lowest subunit IV_D consists mainly of weathered volcanic glass and reddish-brown crescent clay coatings (limpid and speckled) with reddish and golden yellow interference colors. It is about 5 mm thick and appears as a yellowish-brownish boundary layer to the underlying Unit V (Figure 7e). The overlying tephra (subunit IV_C) also consists of a light grey silty sediment and comparatively fresh volcanic glass. This is followed by a tephra layer (IV_B) containing larger charcoal fragments (up to max. 2 cm in diameter) and dark and light phytoliths. In addition, several slightly displaced and non-continuous laminations (graded bedding) of volcanic glass can be observed (Figure 5d). The uppermost subunit (IV_A) is again a mix of slightly rounded volcanic glass, mineral particles, and brownish sediment granules, with a comparable high porosity. The speckled micromass of this unit has a mostly undifferentiated b-fabric, while a stipple-speckled b-fabric is present exclusively in subunit VI_D.

4.1.7. Unit III

The predominant anthropogenic Unit III is characterized by several layers of brown silty sediment, rubified silty sediment, and pale white lateral spreading lenses, which can be identified as tephra. The unit can be subdivided into six subunits, in varying thickness within the thin sections SOD_1-3, SOD_1-4, SOD_3-2, SOD_3-1, and SOD_3-2. The

components seem mixed and reworked. Coarse components consist of obsidian artifacts, slightly rounded trachyte, feldspar minerals grains, rounded clay, and silt granules. In addition, there are a few charcoal fragments, very few slightly burned bone fragments, crust aggregates (silty clay, finely graded bedding), and a high abundance of single phytoliths (dark and light) as well as partly articulated to completely disarticulated phytoliths.

In the field, the boundary to the lower tephra layer (Unit IV) is very smooth, with an almost steady increase in reddish-brown sediment. The sediment appears reworked, indicated by passage features, incorporation of the sediment from Unit IV, and the fact that the coarse features are not positioned horizontally. The lowermost subunit (III_F), seen in thin section SOD_3-2, can be addressed as a transitional zone between the lower subunit (IV_A) and the following anthropogenic unit. It consists of volcanic glass that is slightly mixed into brownish silty clay sediment. Several tephra lenses (III_E) appear randomly. They are affected by disturbance and show signs of lateral spreading (Figure 5c). Towards the top, the content of brownish sediment, as well as amounts of brownish clay coatings, increase. In the upper subunits (III_B, III_C), highly weathered and fragmented volcanic glass with brownish-red hypocoatings in vacuoles (intergranular pores) is still present. Subunit III_B and III_C are characterized by phosphatic features, lateral spread of charcoal fragments, dark and light phytoliths, and undefined fragments of fruit seed coats/seed shells. Furthermore, clusters of spherical phytoliths are found within subunit III_B, with high transparency or masked by dark organic-rich material (Figure 8b). This unit has a light brownish dotted micromass with an undifferentiated b-fabric, which is especially prominent in subunit III_B. Disturbance of the sediment, fragmentation of features, and sediment infilling in channels can be observed. The thin uppermost Unit (III_A), a transition area to Unit II, is characterized by brownish autogenic clay coatings around pumice fragments. The coatings are optically isotropic or anisotropic with very low interference colors and mostly without lamination. Their color varies from yellow to bright brown due to the presence of organic pigments or iron oxides. Pedofeatures such as passage features, borrows, and silty clay infillings are included in all subunits, especially within the two uppermost subunits III_B and III_C.

4.1.8. Unit II

The geogenic Unit II, consisting of two subunits, is well preserved in the excavated profiles and visible in the thin sections SOD_1-1, SOD_1-2, SOD_1-3, SOD_2-1, and SOD_2-2. Even though there is the transition layer (III_A) to Unit III, the boundary is abrupt (Figure 5b). The lower subunit II_B consists of almost pure volcanic glass particles, with a few darker sediment clasts. The upper part of this subunit is compacted and capped by a thin clay-rich crust (II_{B2}), which is only preserved in SOD_1-3 and has been partly eroded and displaced by the overlying subunit II_A. Fine crust fragments are also found in subunit II_A, within the thin section SOD_2-2. This reddish yellow layer II_{B2} consists mainly of weathered volcanic glass and authigenic clay coatings, which are present along the voids and chambers. The upper subunit II_A consists of volcanic glass, sediment granules, burned plant material, and weathered trachytic rock fragments. Some of the coarse components show a brownish coating (armed pyroclasts [50]). The micromass of this unit has an undifferentiated b-fabric. Pedofeatures, such as bioturbation and redoximorphic nodules, are found in the subunits II_A and II_B.

4.1.9. Unit I

The surface Unit I can be divided into two subunits represented by thin sections SOD_1-1 and SOD_2-1. The subunit I_B is a transitional layer between the lower tephra and the surface unit (Figure 5a). Within the brownish silty sediment, weathered volcanic glass and laminations are visible, as well as clay coatings and horizontally oriented and approximately parallel channels. The proportion of organic matter and the degree of weathering of the volcanic glasses increases with height within the upper Unit I_A. The brownish micromass has an undifferentiated b-fabric. Coarse components are trachytic

rock fragments and pieces of charcoal. Biogenic features are passage features and botanic remains (root residues, phytoliths, seed coating fragments).

4.2. Black Carbon Contents and Quality

Fire residue input was quantified by black carbon (BC) content as calculated from the yields of BPCAs.

4.2.1. Profile F35

The BC contents vary across the stratigraphy of profile F35, ranging from <0.01 to 1.53 g BC per kg sediment (Table A1), with three samples peaking in Units I, III, and V. Moderate BC amounts are found in Unit II and the upper part of Unit III, whereas the remaining samples display BC contents near or below the detection limit. The B5CA/B6CA ratios range between 0.59 and 1.28.

4.2.2. Profile G35

BC amounts range between 0.17 and 0.97 g BC per kilogram sediment (180–1579 g BC per kg C_{org}) (Table A1). Within the profile, elevated BC contents occur in the upper part of Unit VII and then decline with depth so that BC contents are comparatively small in the lower part of Unit VII, VIII and IX. The B5CA/B6CA-ratio ranges between 0.76 and 0.85 with one distinctive peak in Unit VII (ratio value: 1.58).

4.3. Phytoliths

In other studies it has already been observed that strongly heated and burned phytoliths obtain a brown to black discoloration or a black core caused by heated carbon inclusions [10,34,35,37]. The phytolith ratio (Table A2) shows that there are dark (burned) and (light) unburned types in almost all samples.

Three categories can be distinguished:

1. The dominance of light phytoliths: Within the samples SOD_002, SOD_027, SOD_060, SOD_103, SOD_106, and SOD_18_03, the light phytoliths dominate, with a rough ratio of ~80:20% of light to dark. The samples originate from geogenic but also anthropogenic sediment units (Units I, IV, VI, VII, VIII). The most common morphotype within the light phytoliths is ELONGATE;
2. Roughly balanced: A rather balanced ratio of ~50:50% (±10%) between light and dark types can be found in the samples SOD_006, SOD_013, SOD_018, SOD_039, SOD_050, SOD_071, SOD_081, and SOD_096. These samples originate primarily from anthropogenic units (III, VII, VIII) and the archaeologically sterile unit (VI). Except for the two samples from Unit III, in which the dark morphotypes are relatively evenly distributed, the ELONGATE morphotype is most common in the other samples, followed by the ACUTE type;
3. The dominance of dark phytoliths: Dark phytoliths, with the three morphotypes equally represented, dominate with a relative ratio of ~5:95% light to dark within the samples SOD_009, SOD_025, SOD_031, and SOD_087. The highest values are found within the anthropogenic sediment Units III and V, followed by a sample from the lower part of the sterile Unit VI. Remarkable is also a high proportion within a geogenic layer that can be associated with the middle section of tephra IV (SOD_025).

The combined results also illustrate differences within the sediment units from which several samples have been examined: The lower two samples of the anthropogenic Unit VII show a higher proportion of light phytoliths (SOD_103, SOD_106), and a balanced ratio within the upper two samples (SOD_071, SOD_096). Variations in the ratio are also observed in five samples of the sterile Unit VI (SOD_039, SOD_050, SOD_060, SOD_071) and Unit IV (SOD_025, SOD_027). Within the predominantly anthropogenic Unit III, the upper sample (SOD_009) shows a higher proportion of dark phytoliths, whereas the samples below show an equal ratio (SOD_013, SOD_018). Even though a lot of well-preserved phytoliths are present within the thin sections, corresponding to Unit IX, the stratigraphically lowest

sample (SOD_18_07) could not be counted due to a high content of fine organo-mineral compounds that were not dissolved during sample preparation.

4.4. Metals in Ammonium Oxalate Extract

The content of Fe_O ranges from 1.77 g/kg to 8.15 g/kg with peaks in the cultural units (I, II, V) and the highest value in the sterile Unit VI (Table A3). The Mn_O values are lower compared to Fe_O, varying between 0.44 g/kg and 2.77 g/kg, with the highest values in the anthropogenic units (I, III, V, and VII). Al_O has the highest values compared to all extracted oxides, with values ranging from 0.77 g/kg in the tephra (Unit II) to 17.07 g/kg in Unit V. The trend of Si_O is similar to that of Al_O, with values ranging from 0.31 to 5.96 g/kg. The highest values occur in Unit V. The ratio of Al_O:Si_O, which is an indicator for the presence of allophane content [51,52], varies between 2:1 (Unit I, VI) and 3:1 (Units II, V).

5. Discussion

The materials and samples investigated in this study represent excavation areas F35, G35, and J29 on the northwestern side of the rockshelter, and therefore a comparatively small area of deposits within the cave. Even though the sediment deposits vary throughout the entire rockshelter, the following interpretation of the micromorphological observations, black carbon (BC) analyses, phytolith ratio, and the AO extractable metals help to understand the general depositional processes and post-depositional alterations as well as the human impact on the deposits.

5.1. Processes of Sediment Accumulation and Post-Depositional Alteration

The following discussion of the depositional processes and post-depositional alterations is based on the new results of the individual units and subunits while considering the preliminary study on site formation based on sedimentological and geochemical analyses by Hensel et al. [1]. The preliminary reconstruction revealed that the accumulation of predominantly autochthonous geogenic, allochthonous geogenic, and anthropogenic deposits in the Sodicho Rockshelter was not uniform and discontinuous [1]. The in-depth microscopic analysis offers new potential for interpreting sedimentary sources and depositional alterations.

The onset of sedimentation within Sodicho Rockshelter is not yet known, as the bedrock has not been reached during excavation. The deepest exposed strata of anthropogenic Unit IX contains stone tool and charcoal fragments and is dated to ~27 ka cal BP [1]. Abundant trachytic clasts and boulders are derived from the trachytic rock walls and the roof (Figure 5h). These trachytic rock fragments contain feldspar crystals in various stages of weathering. Generally, minerals are subject to weathering, especially under a given tropical climate, which typically increases alteration rates [53]. This is also the case within the deposits of rockshelters, as within Sodicho Rockshelter, which are at least partly exposed to the climatic conditions outside of the shelter. A variety of alkali feldspar mineral grains in the sediment groundmass represent the phenocrysts weathered from the fine ground matrix of the trachyte. Fine-grained feldspar alters into clay minerals, such as kaolinite, illite, or vermiculite [53,54]. At Sodicho, this can be observed by the destruction of trachytic rock. Microscopically, Unit IX appears mechanically loosened, and the coarse components are mixed with aggregates of a finer brownish matrix with a high content of organic matter. The disturbance is most probably due to human impact. Furthermore, biogenic pores point to bioturbation as a post-depositional influence. Fragmented aggregates with finely graded bedding suggest deposition by low energy sheet-flow, capable of transporting and reworking fine grained material. Here, sheet-flow is described as a probable slow movement of sediment down the slope, initiated by water entering the shelter through fissures in the walls and ceiling.

The following multi-layered Unit VIII illustrates a series of different geogenic depositional processes, which in turn are interrupted by post-depositional alteration, as in slight bioturbation and unweathered tephra layers, which are intercalated with strongly

weathered deposits (Figure 5h). As an example, the individual volcanic glass particles within a brown matrix (subunit VIII_C) and the two thin layers of almost exclusively volcanic glass indicate tephra that was moved by eolian transport and subsequently relocated by possible sheet flow. The latter is indicated by a few sharp-edged volcanic glass particles in a brownish silty layer, separating two thin layers. Clay coatings with distinct stipple-speckled limpidity, as well as grano- and porostriated b-fabric of the micromass within the subunit VIII_B, illustrate highly weathered tephra (Table S1). Subunit VIII_A is comparable to subunit VIII_C in its composition and features. However, this fine layer shows signs of disturbance due to the influence of water (sheet flow). The input of macroscopic anthropogenic material (e.g., lithics) within Unit VII refers to a human impact on subunit VIII_A as well. The phytolith ratio is characterized by a high proportion (~83%) of light phytoliths (Figure 9) that most likely entered the shelter together with the tephra. Thus, they are representative of the local or regional vegetation outside of the rockshelter, which was obviously not subject to fire. This thin geogenic unit is located chronologically between the two dated anthropogenic Units IX (21–27 ka cal BP) and Unit VII (13.5–18 ka cal BP) [1] and thus still in the time range of the LGM. Any signs of anthropogenic habitation within this very thin tephra are missing, indicating that humans were absent from the rockshelter.

The deposits in the thin sections of the predominantly anthropogenic Unit VII seem to be disturbed mainly by biogenic activity (abundance of biogenic pores) and human action, indicated by anthropogenic finds. A further cause of the disturbance could have been the impact of the trachytic boulders of the rockfall layer. The partial collapse of the ceiling may be caused by an increased water impact on fissures in the ceiling, related to the onset of the AHP. Macroscopic changes within the sediment sequence were observed during excavation, e.g., lenses of weathered tephra in excavation square G35 (Figure 3). Furthermore, dotted brownish coatings are found, which may be masked by organic material (humus) [10]. Based on the micromorphological observations, no further subunits could be distinguished for this unit. However, the geochemical analyses show increased magnetic susceptibility and higher values of Mn and P (Figure 4) in the upper part of the unit [1], which correlates with higher values of dark phytoliths (sample SOD_081 and SOD_096). This shows that the human influence and burning activity is more pronounced in the upper part of the unit. Light-colored phytoliths are predominant in the sediment samples of the lower area. We suggest that dark-colored phytoliths indicate that these were introduced by humans due to fire activity.

A mixture of autochthonous and allochthonous geogenic sediment is common in Unit VI, the deposit dated to the African Humid Period [1], a phase characterized by increased precipitation but also including short dry periods [55–58]. Previous geochemical and sedimentological studies revealed a high influence of weathering, with an increased clay content, characterized by a lower K/Rb ratio (weathering ratio) and increased Fe_2O_3 [1]. The ammonium oxalate extraction of the study at hand verifies this observation. A direct comparison of the corresponding curves of Fe_{XRF} and Fe_O clearly indicates higher contents of Fe and increased precipitation of amorphous pedogenic iron (hydr)oxides within the archaeologically sterile Unit VI (Figure 10). Here, the total Si content (XRF) is very low and Si_O content low to moderate, caused by the increased influence of precipitation in the highlands, associated with increased weathering and leaching of Si within the sediment [6,59]. Formation of halloysite or kaolinite at Sodicho is likely, indicated by Si leaching.

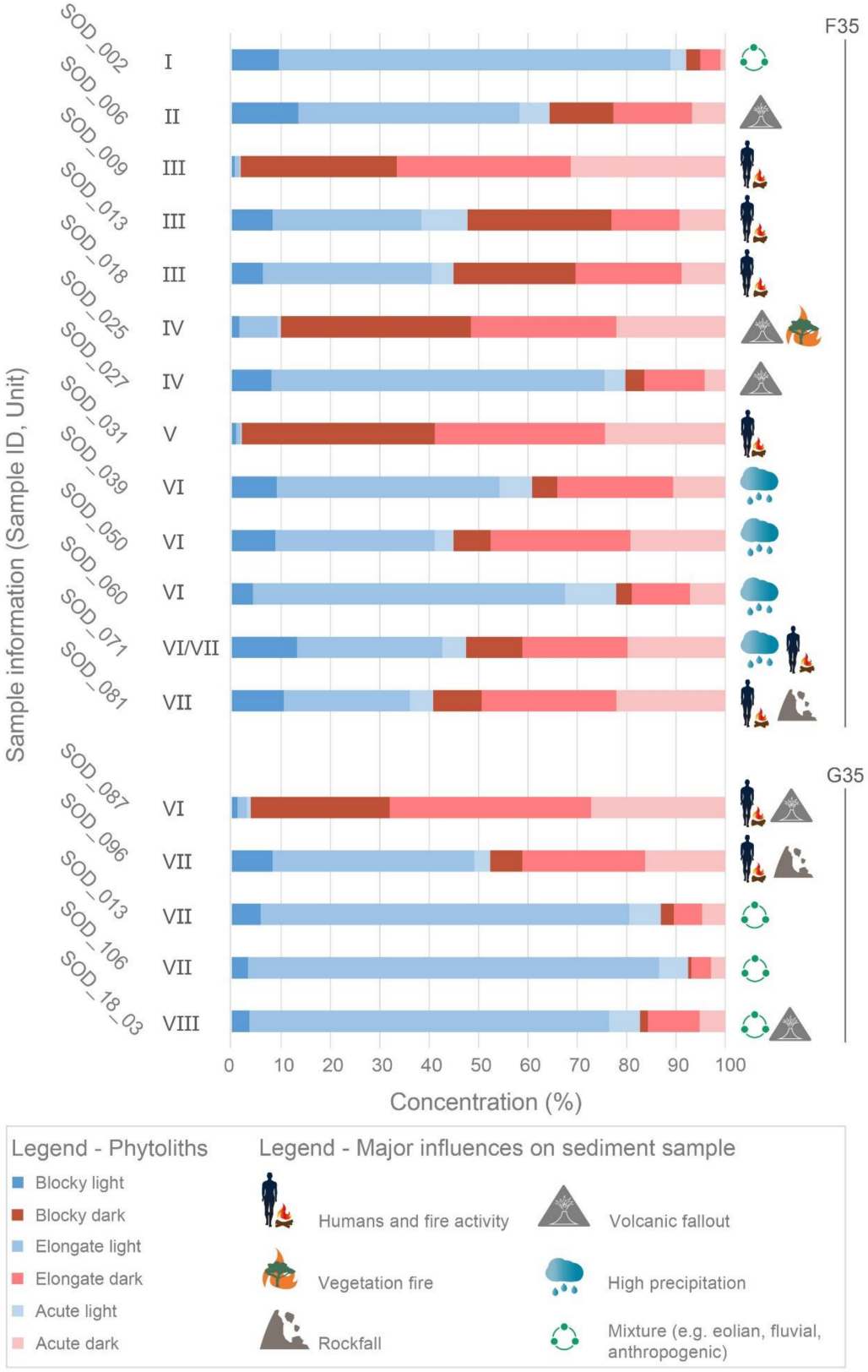

Figure 9. Interpretation of influences on sediment samples and phytolith ratio: sample counts of dark (burned; red) and light (unburned; blue) in percentage. Samples are arranged based on the stratigraphic position of the sedimentological units (roman numbers) for both excavation square F35 and G35. The depth of each sample can be found in Table A2.

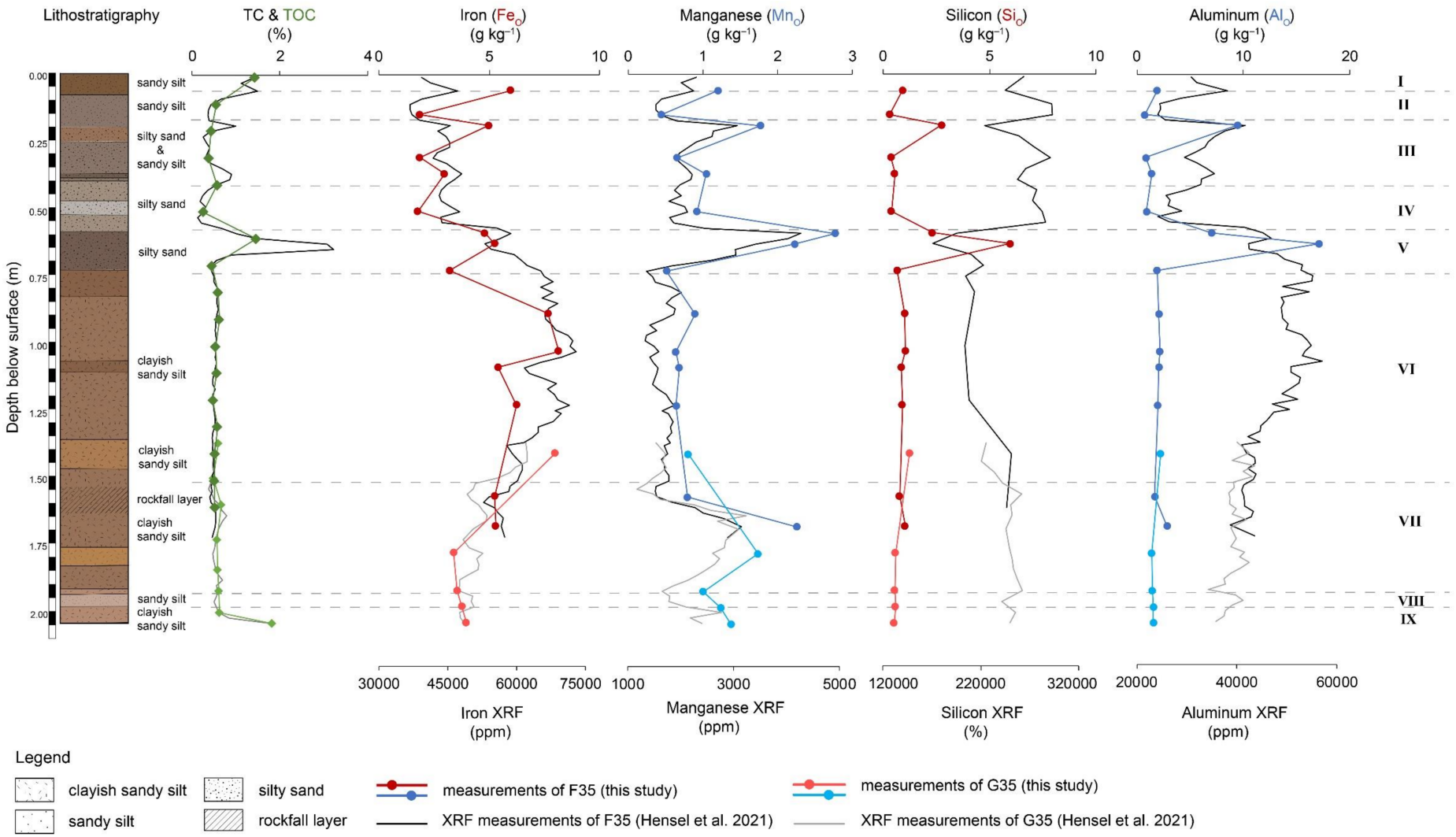

Figure 10. Comparison of new results of the oxalate extract of Fe_O, Mn_O, Si_O and Al_O (colored graphs) with the geochemical results from Hensel et al. [1]: carbon content (TC and TOC), total values of Fe, Mn and Al determined with a portable XRF and Si with XRF (black-grey graphs) (mod. [1]).

Micromorphological investigations identified five subunits of Unit VI. They probably represent different phases with changing moisture conditions during the African Humid Period. The lowermost subunit VI_E represents strongly weathered tephra in the shape of accommodating aggregates (Figure 8g). The aggregates contain volcanic glass in a clayey micromass with a bright interference color. The formation process of this layer probably occurred through several successive steps. It is possible that the volcanic ash was blown into the rockshelter and was redeposited by low-energy sheet flow, evident in the silty graded beddings within subunits VI_{E2} and VI_E in.

The Al_O:Si_O ratio, with a value of 1.78:1 (Table A3), is comparatively narrow within the heavily weathered subunit VI_E. The weathering process of the silicon-rich tephra has progressed so far that more stable secondary clay minerals such as halloysite or kaolinite could have formed. These clay minerals, with a similar aluminosilicate composition and bright interference color, have a Al_O:Si_O ratio of 1:1 and generally tend to form in silicon-rich environments [6,60]. As sediment from subunit VI_D is found in the gaps between the aggregates, the redeposition of the tephra most probably took place during the deposition of subunit VI_D. Considering the phytolith ratio of two samples (SOD_071, SOD_087) derived from subunit VI_E, a dominant proportion of dark phytoliths is noticeable in sample SOD_087, further illustrating the taphonomic processes that altered the sediment between the tephra aggregates and influenced local phytolith composition. Thus, the dark phytoliths result most likely from translocated anthropogenic combustion features associated with past occupation (Unit VII). Subunit VI_D also shows signs of mechanically disturbance, with rounded sediment granules and aggregates and fragmented limpid clay coatings. Volcanic glass is most likely weathered and is very rare.

Changes in moisture availability during the AHP are evident within the subunits VI_C, VI_B, and VI_A through shrink and swell processes and disturbed sediment aggregates, as well as the possible formation of Fe-(hydr)oxides (e.g., goethite) coatings along voids and channels, due to temporal dehydration [61,62]. Increased Fe levels in rockshelter deposits have been related to the high anthropogenic input of organic matter, which later decomposed [63]. Organic matter contents of Unit VI at Sodicho are not increased, and there are no further indications (e.g., artifacts, charcoal) that humans were present during the accumulation of this unit. We thus assume that Fe was enriched in Unit VI in the course of silicate weathering in- or outside of the rockshelter. Altered iron oxides, such as the association of hematite and goethite, are common for alteration in a tropical environment in acidic sediment [6], conditions similar to those at Sodicho. Here, yellow, homogenous clay coatings are directly overlain by banded radiating, acicular Fe-(hydr)oxide needles in samples SOD_7-1 and SOD_7-2. Such combined layers of clay (often kaolinite) and goethite are known to develop a boxwork fabric (network structure) or even a fanlike intergrowth [10,64,65] but their genesis is not completely clarified. At Sodicho, the well-crystallized Fe-(hydr)oxide needles illustrate the advanced stage of weathering, which led to an increased release of Fe and a subsequent development of the needle structure. In other cases, the presence of Fe-(hydr)oxides also indicates a development under water unsaturated (vadose) conditions and is therefore indicative for temporal dehydration of the sediment [61,62].

The subaqueous deposition is indicated by layers and aggregates with graded bedding of silt and clay particles [66]. Redoximorphic pedofeatures such as Fe/Mn nodules, reddish-brown staining and hypocoatings, and especially the abundance of clay lamination are signs of the influence of water [67,68]. These mentioned indicators are found within subunit VI_C. It is likely that precipitation was extremely high over longer periods of time. Thus, the water could not drain quickly enough or percolate through the sediment, leading to an accumulation of water in shallow pools and possibly complete waterlogging. By using a Predictive Vegetation Model, linked to a Lake Balance Model of lake Chew Bahir, the recent study by Fischer et al. [69] determined an increase in moisture availability of 25–40% during the AHP, compared to today's values. This observation of increased moisture conditions emphasizes calm water deposition at Sodicho for this time period.

But, these deposition conditions were interrupted by phases of disturbance. Reworked sediment layers within the same Unit VI are probably caused by shrink and swell processes, as indicated by fragmented and contorted aggregates, especially within the subunits VI_C and VI_B in the thin sections SOD_7-1 and SOD_7-2 (Figure 5f). Very similar observations were made in the lower most and archaeologically sterile unit of Wonderwerk Cave in southern Africa [66]. In addition, to the shrink and swell processes in Unit VI, an abundance of biogenic pores points to a disturbance by bioturbation. Mesofauna (0.1–2 mm) probably used existing physical voids and actively modified them by, e.g., enlargement, as described for structure-formers [70].

The phytolith ratio of the samples from Unit VI shows a relatively balanced value of light and dark morphotypes (except for sample SOD_60 with dominant light phytoliths). For this unit, we suggest that the phytoliths were brought naturally by eolian processes or sheet flow into the site and thus reflect the past natural environment. Since this unit is archaeologically sterile, an entry by humans can be ruled out. Therefore, the dark phytoliths could derive from vegetation fire ignited by hot volcanic ash fall. The identified depositional processes of this unit are evidence of the abandonment of the shelter due to extremely wet and uninhabitable conditions during the AHP.

According to the previous geoarchaeological studies at Sodicho Rockshelter, the anthropogenic influence increases again at around 4.7 ka cal BP [1], corresponding with the probable termination of the African Humid Period in this region [55]. Micromorphologically, this is indicated by the occurrence of obsidian artifacts, charcoal, and other fire residues within thin section SOD_I-1-2 from Unit V. Likewise, the high abundance of dark phytoliths (~98%) indicates human occupation and intense fire activity. A further interruption of human occupation coincides with an increase in water influence on the deposits, as seen in the redistributed fragments of limpid clay coatings and tephra lenses (V_{A2}) with graded bedding and rounded volcanic glass particles in subunit V_A.

The elevated values of the two manganese curves (Mn_{XRF} and Mn_O) (Figure 10) within this and also the other anthropogenic layers probably indicate the decay of organic matter or inorganic compounds that accumulated during human occupation [1,63]. This correlates with increased TOC values and increased amorphous organic matter in the groundmass. The Al_O values are particularly high in the uppermost part of Unit V, where geochemical observations proved a high BC (Figure 11) and TOC content. The absorption of Si by Al-oxides could explain the high Si content in the anthropogenic units. The increase in the Al_O:Si_O ratio (~3:1) within the anthropogenic units (Figure 11) suggests a possible formation of allophane or imogolite. A large part of released Si may thus be converted to secondary silicates, but this did not result in the accumulation of total Si, which is depleted in anthropogenic Units V and III relative to other layers. However, other studies showed that Al is more easily incorporated into organic complexes than it is available for allophane or imogolite formation [6,60]. For Sodicho, it appears thus more likely that the increased Al_O originates from metal-organic matter complexes.

The following Unit IV is composed of lighter colored tephra, thus allochthonous geogenic deposits that deposited relatively abruptly. This tephra is only exposed within the excavation square F35 and is not visible in square G [1]. The main proportion of the tephra (Unit IV) entered the rockshelter via eolian transport during an initial phase of deposition. A coarse monic microstructure with homogeneous composition of sharp-edged volcanic glass particles within subunits IV_C illustrates this (Figure 8g). Evidence of increased moisture and weathering intensity can be found in the highly weathered subunit IV_D with golden yellow colored clay and a stipple-speckled birefringence (Figure 7e). An Al_O:Si_O ratio of 2:1 suggests the presence of imogolite-like or proto-imogolite allophanes [6,71]. Indications for this formation, based on an undifferentiated b-fabric, i.e., the absence of interference colors, are found in this less-weathered subunit.

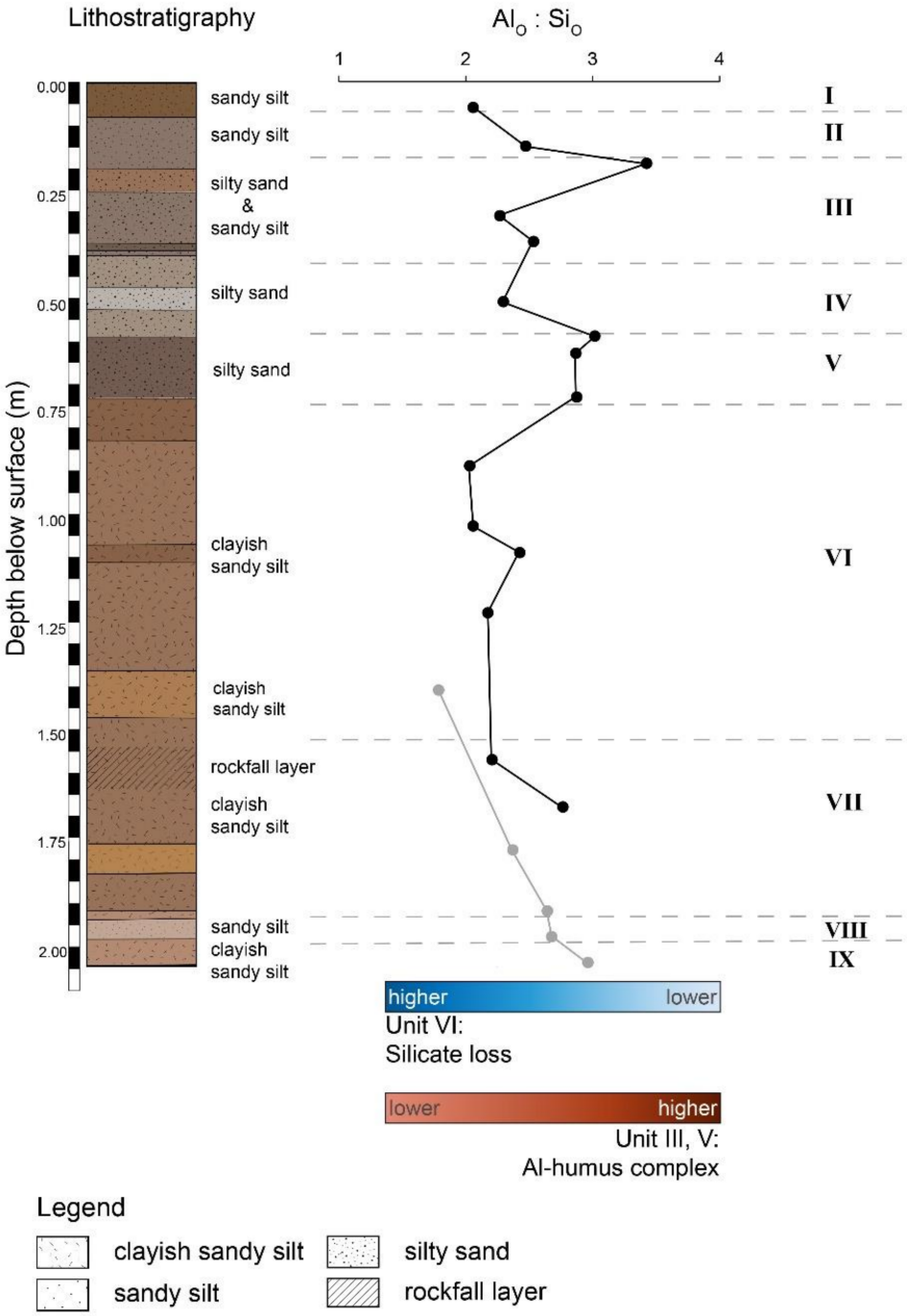

Figure 11. Illustration of the discussed factors (silicate loss; Al-humus complex formation) affecting the Al_O:Si_O ratio and allophane estimation for Sodicho. Silicate loss is accompanied by the formation of clays in Unit V. Formation of Al-humus complexes in the anthropogenic layers.

Subunit IV_B shows indication for redeposition of the tephra by low-velocity flow, as in intermixing fine brownish gradations rounded volcanic glass, partial compaction, graded bedding, rounded sediment granules, as well as bigger and slightly fragmented charcoal pieces (Figure 5d). These investigations of slow-moving fluvial deposition can be compared to observations at the nearby Mochena Borago site. In this context, the observation of fine brownish lamination within the Yellow Brown Tephra (YBT) can be attributed to low-energy flow and accumulation in small water pools [2]. Comparison between Mochena Borago and Sodicho Rockshelter illustrates comparable depositional settings, influenced by changing moisture availability on a millennial scale, even though there is a temporal offset between

the two sites. The phytolith sample SOD_025 corresponding to this subunit contains about 90% dark phytoliths, in contrast to the sample (SOD_27) corresponding to subunit IV_C that contains only 20%. Given that the bigger charcoal pieces and a high proportion of dark phytoliths are preserved in the middle of a purely geogenic layer, they most probably indicate non-anthropogenic burning events, such as natural forest or bush fires [68,72], initiated by hot gas clouds or lava flow.

The following settlement phase (Unit III) can be radiocarbon dated to 2.1 to 1.8 ka cal BP [1]. The micromorphological observations revealed a rather smooth transition (subunit III_F) with increasing evidence of human occupation. The upper parts of the unit (III_B and III_C) are bright reddish in color and more cemented than the lower parts of the unit. Subunit III_B has a dark-brownish-colored groundmass due to higher organic content. The Al_O:Si_O ratio has its highest value in this subunit, indicating a high proportion of Al-humus complexes. The typical features observed in the previous anthropogenic units, such as stone artifacts and evidence of fire residue, are further discussed in Section 5.2. Three phytolith samples derived from subunits III_D (SOD_018) and $III_{B/C}$ (SOD_013, SOD_009) reflect the pattern of elevated geochemical values in this unit (Figures 4 and 10). Thus, an abundance of burned phytoliths in the upper part of the unit indicates intensified human impact. As a result of human activity on the former surface, such as the digging of pits, construction of hearths, and probably site maintenance, the deposits of subunit IV_A were partly incorporated into Unit III. This is particularly apparent from the large proportion of volcanic glass in the lower part of the unit (III_F and III_D) and from the laterally distributed tephra lenses (III_E) in F35 (Figure 2). Despite the post-depositional disturbance and slight compaction, the lenses are micromorphologically similar to tephra from Unit IV in terms of groundmass color, size of volcanic glass particles, brownish sedimentary granules, and occasional non-continuous laminations. The uppermost subunit III_A can be described as a transition layer, despite the sharp color distinction between Unit III and II. Here, the transition was not smooth from one unit to the other, as observed between Units IV and III. It consists of bioturbated sediment, in which parts of the brownish silty and clayey sediment from Unit III are incorporated into the channels, borrows, and chambers of the tephra in Unit II

The following Unit II is divided into two subunits, with the lower subunit II_B as light-colored tephra, which was introduced by eolian transport. Within the sample SOD_1-3, a yellow crust of clay and silt (subunit II_{B2}) with a few slightly rounded volcanic glass particles overlay the slightly compacted upper part of subunit II_B (Figure 8g). Here, compaction is interpreted as the result of water dripping from the rockshelter ceiling. Laboratory studies have shown that structural surface crusts with reduced porosity and reduced permeability can form on tephra during a phase of stable surface conditions under simulated rainfall [73,74]. At Sodicho, this crust on top of subunit II_B is an indication of a rather stable surface. The features of reworking (e.g., intermixing with sediment aggregates) in the overlying tephra II_A illustrate remobilization of the sediment. Simultaneous degradation of the yellowish clayey crust is possible (Figure 8h). Given that the subunit is subject to bioturbation, this process also contributed to the destruction of the crust. The phytoliths in subunit II_A (SOD_06) were transported into the rockshelter together with the tephra and represent the vegetation outside.

The onset of the predominantly anthropogenic surface Unit I, and thereby the most recent occupation, is indicated by a transition to brown and organic-rich sediment with limpid clay coatings, fine charcoal fragments, and indicators of mechanical disturbance (subunit I_B). Within subunit I_A there are well preserved biological components such as roots and seed coat fragments. Indications for bioturbation as in passage features are present throughout the entire Unit I. Thus, partly intermixing with geogenic subunit II_A was observed. This explains the presence of ~35% dark phytoliths in the sediment samples corresponding to subunit II_A. In contrast to this, a phytolith ratio with 90% light phytoliths indicates the decreasing presence of humans in this young (250–400 cal BP) sediment Unit I.

5.2. Human Behavior and Fire Activity at Sodicho

Identifying human activity and interpreting human behavior in a micromorphological context is fundamental for the study of archaeological sediments [75]. With the help of the applied methods, in-depth insight into the behavior of prehistoric humans can be provided, especially with regard to the use of fire. Combustion features at archaeological rockshelters not only speak for starting and controlling of fire but also indicate the need for light, heat, and of course, the use of the fire for food preparation as kind of a short-term human activity event [18,49]. At the Sodicho Rockshelter, evidence of human activity can be seen macroscopically by hearths, pits, and lithic artifacts [1]. The most prominent indirect evidence for burning at Sodicho is the abundance of charcoal fragments within the anthropogenic units. Microscopic evidence of reworked fire residue, such as charcoal (fragments), slightly burned or even calcined bones, as well as rubification of sediment, was observed in almost all anthropogenic units. Slightly burned and calcined bone fragments can either indicate that fires at Sodicho were used for food preparation and/or that the bones were used as burning material. It is also possible that bone fell into the fire by coincidence or that it was disposed of as waste. Three parted combustion features, including ash, charcoal, and rubified sedimentary layers, are apparent within two slightly disturbed hearths in G34 (south) and G35 (south) (Figure 2), which were not sampled for micromorphology. Carbonate ash layers, a typical overlying by-product of burning [49], are not contained in the thin sections from Sodicho. This means that decalcification occurred, influenced by the dissolution of acidic trachyte bedrock of the rockshelter. Decalcification is often associated with the formation of Al phosphates in clay-rich sediments [49,76]. In Sodicho, these elevated Al values correlate with increased phosphates values [1]. These observations strengthen the assumptions that reworking and leaching processes took place at Sodicho. Evidence of fire residue is particularly evident in sample SOD_I-1-1 in Unit V, which exhibits the mentioned features above a relocated and partially eroded tephra (Figure 5e). Slightly burned bone and calcinated bone fragments that had not been visible macroscopically [1] are included as single fragments or as larger coherent fragments, suggesting a slight displacement (Figure 7a). Dark matter at the lightly burned bone fragments within subunit V_A can be interpreted as char [11,49,77]. The displacement and fragmentation of sediment in anthropogenic layers of Sodicho reflect trampling and rake-out (sweep-out) processes in the center or around a fireplace, scattering the burned material laterally and intermixing it with unburned material as described by various authors [49,78]. This is also indicated by rounded aggregates of the rubified sediment and the oblique truncation of the tephra. Whether this light-colored tephra was previously relocated by humans or even intentionally dumped into a pit cannot be clarified at this point of the research. However, it is obvious that the tephra does not seem to be in-situ at this position, as the edges of the layer appear angular in profile F35 North (Figure 3). In addition, fine charcoal particles and distorted sediment aggregates are included. This means that the origin of the bright tephra is unknown, as no comparable tephra layer has been excavated at this stratigraphic level before.

According to other studies, the rubefaction of sediments depends on the organic and mineralogical composition of the substrate, the sediment moisture, and the duration of burning [49,79]. There are two types of rubification within the anthropogenic units of Sodicho. First, there is reddening activity caused by the oxidation of Fe^{2+} to Fe^{3+} and the development of iron oxides (such as hematite) [49,80], which is connected to anthropogenic fire, observed in the sample SOD_I-1-1 in Unit V. Secondly, reddening appears in Unit III, probably due to the combination of human fire activity and the alteration of volcanic glass. According to the study of Ferralsols of the Canary Islands analyzed by Rodríguez-Rodríguez et al. [81], discussed in Stoops et al. [50], volcanic glass alters into a yellowish isotropic product. With increasing alteration, the destruction and fissuring increase, followed by a rubification with dark red optically isotropic alteromorphs. Within the thin sections from Unit III (such as SOD_3-1), increased fragmentation and red brownish coatings are present in vacuoles of the volcanic glass. In addition, red-colored humic

Nitisols, the typical soils of the region, occur outside of the shelter. It seems possible that this red soil material (clay and silt size) has been transported from outside into the Sodicho Rockshelter by low energy sheet flow or through fissures in the rockshelter walls and incorporated into the archaeological sediment [1] as assumed for other rockshelter sites [49,72,82–84].

As previously mentioned, charcoal is found in all human-influenced units. The question arises whether we can detect differences in fire use between the units, and thus temporal differences, that may indicate changes in human behavior. For this purpose, we use the information from the BC analyses and the phytolith ratio, as well as the results of sedimentological and geochemical analyses by Hensel et al. [1]. The BC content, as a proxy for fire residue input, correlates with the increased MS and Mn values in the anthropogenic Units III, V, and VII (Figure 12) and thus complements the findings of charcoal, burned bone, and calcinated bone fragments.

The absence of BC in the preferentially geogenic units can therefore be seen as an additional indication for the absence of humans since the BC particles would have been distributed within the rockshelter even if the inhabitants used fire in another part of the shelter. At the same time, the higher fire activity in these occupation periods was accompanied by an increased degree of BC condensation due to higher fire temperature, as indicated by comparatively low B5CA/B6CA ratios. This is particularly useful when aiming, for instance, at distinguishing hot hearths with low ratios of penta- to hexacarboxylic benzoic acid (B5CA/B6CA) from cool vegetation fires, e.g., natural grass or forest ground fires, with higher B5CA/B6CA ratios [33,85,86]. Thus, the BPCA ratios from Sodicho support other indicators of anthropogenic fire, such as burned bone fragments and stone tools, providing evidence for food preparation [87]. Lower B5CA/B6CA ratios and thus comparatively higher temperatures are found within Unit III, which has been dated to a period of 1.8–2.1 cal BP. The older Unit V (4.3–4.8 ka cal BP) shows slightly higher ratios, especially when samples with low BC values are included. By comparing these observations for the defined units with the results of the phytolith ratio, it is noticeable that the upper sample in Unit III (subunit III_B) shows only a slightly higher proportion of dark phytoliths compared to the values in the other anthropogenic units. Within both units, a strong abundance of dark phytoliths is found (~98%). Therefore, no difference in human fire intensity can be determined based on the counting of phytoliths alone. However, the abundance of discoloration in phytoliths is without doubt caused by burning activity, as it is more pronounced in units containing fire residue features.

Unit III shows a phosphate-rich groundmass with preserved fire residue, such as charcoal and black char with a vesicular structure, supporting the hypothesis of the use of wood as a fuel. However, the large proportion of dark phytoliths of the ACUTE morphotype in sample SOD_009 indicates that grass was used as a burning material as well.

Small transparent phytoliths, identified as SPHEROIDAL ORNATE, are found in great abundance in Unit III (Figure 8b). These also occur in Unit V, but to a much lesser extent, and individually or in cell association in the areas of combusted matter. SPHEROID ORNATE phytoliths with an irregular surface are common in monocots and woody dicots [88]. In our thin sections, SPHEROID ORNATE occurs in cell clusters which likely are parts of seeds (Figure 8b) but were not observed during phytolith analyses. This is due to the close cell association which was not dissolved during sample preparation.

The phosphate-rich groundmass in Unit III correlates with elevated phosphate values, determined by X-ray fluorescence (XRF) (Figure 4) [1]. Due to poor bone preservation, with the exception of small bone fragments identified in the thin section, no definite conclusions can be drawn regarding the use of the rockshelter by animals. Phosphate can be introduced in various forms, such as human activity, bird guano, or excrements [76]. Since the human-influenced units were partly reworked, a biogenic input could be possible as well. Although the origin of the phosphorus cannot be unambiguously clarified, Unit III represents a settlement phase based on our sedimentological and geochemical findings as well as the occurrence of archaeological artifacts.

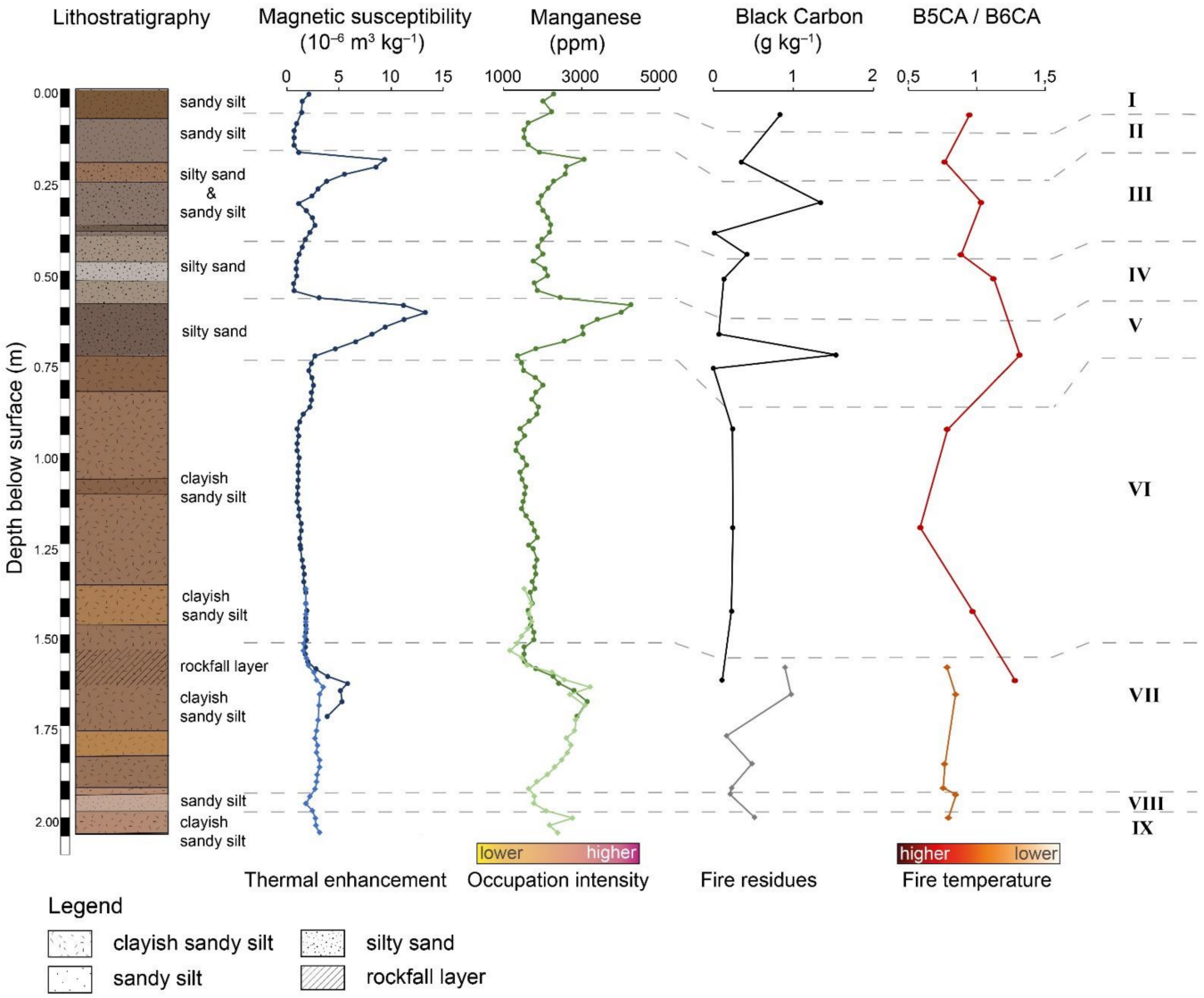

Figure 12. Comparison of the new BC results with the geochemical results from Hensel et al. [1]. Geochemical properties of the profile F35 and G35 (left to right): lithostratigraphy according to grain size analysis and sediment color measurement; magnetic susceptibility; manganese value (mod. [1]); BC content; B5CA/B6CA ratio values; sedimentological units. Grey dashed lines indicate association to the units. Note that the lines of BC content and B5CA/B6CA ratio values are staggered because the samples were taken from two excavation squares (F35 and G35).

The questions arise, whether the limited evidence of a changing fire temperature could have been caused by degradation or even leaching and, therefore, how the degree of weathering can affect the preserved information in the archaeological deposits. It is noticeable that BC and the phytolith ratio peaks within the upper anthropogenic units (III and V) and that no micromorphological features were observed within these units that could indicate the mentioned extreme weathering processes as observed in Unit VI, corresponding to the AHP. Furthermore, no trend between the BC content and increasing depth or sediment age was detected, which makes distinct pedogenic processes such as percolation by water less likely in the anthropogenic units.

6. Conclusions

The combined results of this study not only confirmed previous geoarchaeological investigations on site formation, post-depositional alteration, and human impact at Sodicho

Rockshelter. In addition, they provide deeper insights into weathering processes and the identification of prehistoric human behavior under shifting environmental and climatic settings. The combination of the different methods allowed a more precise subdivision of the units and the determination of individual depositional processes. In particular, the intercalated tephra layers display a clear interruption of human occupation at Sodicho. Given the high proportion of weathered and unweathered volcanic glass particles within the entire stratigraphy, we cannot clearly determine the allophane content, but we assume a partial allophane (proto-imogolite), imogolite, and even halloysite and kaolinite formation, respectively. Furthermore, clay minerals are formed by the weathering of the local trachytic bedrock but could also have been washed in from outside as clayey soil material [1].

Significant changes in moisture conditions on the substrate and the associated impact on depositional and post-depositional alteration processes (e.g., sheet flow, shrink and swell processes) are especially pronounced during the conditions of the AHP. On the other hand, bioturbation partly disturbed the original stratification of the deposits and therefore affected the preservation of environmental and archaeological information. The depositional processes identified for the AHP verify that the rockshelter was abandoned at this time, probably due to wet and uninhabitable conditions. In contrast, the combination of the archaeological finds and the microscopic evidence from layers dated to the time range of the LGM [1] verify that humans visited the rockshelter repeatedly.

Human occupation contributed significantly to site formation and post-depositional disturbance of the sediment. The microscopic identification of calcined and slightly burned bone fragments within fire residue and indications for trampling (compaction and bone fragmentation), dumping activity, and site maintenance verify that inhabitants of Sodicho were able to start, maintain and control fire. The combination of micromorphological observations and BC analyses yielded consistent results and thus allowed the identification of temporal changes in fire activity. Consequently, changes in BC contents and composition are interpreted as changes in the human-induced input of fire residues. It was not possible to differentiate fire intensity between the anthropogenic units based on the phytolith ratio. However, the combined analyses allowed the identification of human fire activity (Unit III, V) and the differentiation of natural vegetation fire (Unit IV) through the abundance of dark phytoliths. Light phytoliths that entered the site naturally provide the first evidence for the reconstruction of local vegetation changes at Mount Sodicho. In conclusion, this case study contributes to the development of comprehensive, methodical approaches to tackle and disentangle challenging stratigraphies in the tropical highlands of Ethiopia.

Supplementary Materials: The following are available online at https://www.mdpi.com/article/10.3390/geosciences12020092/s1, Table S1: Electronic Supplement: Overview of micromorphological results.

Author Contributions: Conceptualization, E.A.H., R.V. and O.B..; methodology, E.A.H., L.W. and K.N.; validation, E.A.H., M.K., L.W., K.N., R.V. and O.B.; formal analysis, E.A.H., L.W. and K.N.; investigation, E.A.H., L.W. and K.N.; resources, E.A.H., M.K., L.W., K.N., R.V. and O.B.; data curation, E.A.H., L.W. and K.N.; writing—original draft preparation, E.A.H.; writing—review and editing, E.A.H., M.K., L.W., K.N., R.V. and O.B.; visualization, E.A.H.; supervision, M.K., R.V. and O.B.; project administration, R.V. and O.B.; funding acquisition, R.V. and O.B. All authors have read and agreed to the published version of the manuscript.

Funding: This research was funded by the Deutsche Forschungsgemeinschaft (DFG, German Research Foundation), grant number 57444011—SFB 806.

Institutional Review Board Statement: Not applicable.

Data Availability Statement: The data presented in this study are available in Appendix B—Results and the supplementary material here.

Acknowledgments: We kindly thank the Authority for Research and Conservation of Cultural Heritage (ARCCH) of Ethiopia for their permission and general support and the Ministry of Mines and Energy for the approval of our export permits. The Deutsche Forschungsgemeinschaft (DFG, German

Research Foundation) supported this research as part of project A1 "Out of Africa—Late Pleistocene Rock Shelter Stratigraphies and Palaeoenvironments in Northeast Africa" in the framework of the Collaborative Research Centre 806 (CRC 806) "Our way to Europe" (grant no. 57444011—SFB 806). We thank K. Greef for guidance and assistance during the oxalate extraction and Th. Beckmann for the preparation of the micromorphological thin sections. We are very grateful to Thomas Albert, Degene Bado, Dejenne Degena, Mesfin Gete, Solomon Gitaw, Habir Mohammed Kebir, Tom Noack, Mareike Röhl, Christian Schepers, Desta Sinajew, Mehdanit Tamerat, Fitsum Tefera, Minassie Tekelemariam, and Thorben Thenbruck for their participation during various field seasons at Sodicho. Finally, we thank the local residents of Mt. Sodicho for their participation and support in field research.

Conflicts of Interest: The authors declare no conflict of interest.

Appendix A. Methods

Appendix A.1. Micromorphology

Microscopic observations of soil and sediment thin sections have been crucial methods since they were established by W.L. Kubiëna in the 1930s to identify the spatial structure of features on a microscopic scale [7,10]. At Sodicho, the sediment blocks were secured with gypsum bandages. The samples from the excavations in 2016 had to be bandaged again with gypsum after a one-year storage phase to ensure further transport to the thin section laboratory. In the process, sample Sodicho_6 was damaged at the upper right edge. This incident was also considered in the analysis and interpretation. The impregnation of the sediment monoliths, as well as the preparation of the <30 µm thick, thin sections, followed the instructions of Beckmann [89]. The description of the thin sections followed the guidelines and terminology of Stoops [10]. The thin sections were flatbed scanned (Canoscan 9000F, Canon) to document the overall composition and to detect subunits on a mesoscopic level [90]. The detailed microscopic examination was carried out with a polarizing microscope Axiolab (Zeiss) and the digital image capture software Axiovision (Zeiss) under plain-polarized, cross-polarized, and oblique incident light.

Appendix A.2. Fire Residue (Black Carbon) Analysis

All samples were dried (40 °C), sieved (>2 mm), and milled prior to analysis. Organic carbon (OC) contents were determined with a Soli TOC Cube (Elementar Analysensysteme, Hanau, Germany) according to Mörchen et al. [91]. Samples preparation followed the protocols of Glaser et al. [32] and Brodowski et al. [31]. Black carbon (BC) content and composition were determined by oxidation of BC to benzene polycarboxylic acids (BPCA). To avoid the contribution of BPCAs from non-pyrogenic matter, the evaluation was limited to five- and six-times carboxylated BPCAs (benzene pentacarboxylic acid and mellitic acid, B5CA/B6CA), and a threshold of 5 mg organic carbon per sample was strictly maintained [92]. While the sum of BPCAs informs on BC quantity (comp. [31,32]), its composition, i.e., the degree of aromatic condensation, provides additional information about changes in combustion temperatures: the hotter a fire burns, the more benzene with 6 carboxyl rings are isolated from the combustion residue (comp. [33,85,93]). Hence, the ratio of B5CA/B6CA was used as a proxy for changes in combustion temperatures [33,85].

Samples were measured using a gas chromatograph equipped with a flame ionization detector (FID; Packard 6890 gas chromatograph, Hewlett Packard GmbH, Waldbronn, Germany), and an HP-5 capillary column (30 m × 0.32 mm i.d., 0.25 mm film thickness, Macherey-Nagel, Düren, Germany; for oven program see Brodowski et al. [31]). Citric acid was used as the first and biphenylene-dicarboxylic acid as the second internal standard to quantify the recovery of citric acid (average recovery: 72%). The BC amounts are expressed relative to kilogram sediment. As proposed by Glaser et al. [32], BPCA yield was corrected for CO_2 loss and insufficient conversion of BC to BPCAs using the factor 2.27, which provides a conservative, minimum estimate of total BC in soil [32]. Note that the B5CA/B6CA ratio was excluded from the evaluation if a sample contained less than 0.10 g BC kg^{-1} as interpretation may not be reliable in this case; this applies to samples BC4, BC7 and BC9.

Appendix A.3. Phytoliths

Phytoliths were extracted from ca. 10 g of sediment from each sample in the laboratory of the Senckenberg Research Institute, Frankfurt, using a modified protocol after Piperno [89] (pp. 90–93):

1. Deflocculation with EDTA;
2. Sieving for removal of coarse sediment and modern plant remains;
3. Clay removal with Stroke's Law gravity separation;
4. Carbonate destruction using HCl;
5. Organic matter removal with HNO_3 and $KClO_3$;
6. Heavy liquid separation with sodium polytungstate.

Small amounts of each extracted phytolith sample were mounted on microscopic slides in immersion oil and counted at 400× magnification. At least 300 phytoliths were counted for each sample. In this study, light stands for the absence of any recognizable fire influence and thus for a light/transparent appearance. In the study by Parr [37], it was observed in experimental fire studies that phytoliths take on a dull and opaque color under oxidative conditions. We subsumed as 'dark' phytoliths those with a complete brown to black appearance as well as those with a dark core. Because our interest in this study was mainly to reconstruct the impact of fire on the rockshelter sediments, we restricted counting to three most conspicuous and common morphotypes, following the nomenclature after Neumann et al. [36], the guidelines of International Code for Phytolith Nomenclature (ICPN) 2.0 [36]:

- ELONGATE (ELO): Rectilinear phytoliths with variable sizes and edges (entire, sinuate, etc.). These phytoliths were observed as single-celled or articulated;
- BLOCKY (BLO): Compact phytoliths with length/width <2 and equal width and thickness;
- ACUTE BULBOSUS (ACU_BUL): Unarticulated phytoliths with a wider antapex that narrows down to an acute apex.

The light and dark samples of each morphotype were counted separately. For each sample, the ratio of light (absence of fire influence) vs. dark phytoliths (contact with fire) phytoliths was calculated.

Appendix A.4. Ammonium Oxalate Extractable Fe, Mn, Al, and Si

Moderate acidic reactions, initiated by acidified ammonium oxalate, are used to dissolve active non-crystalline oxides, organically bonded oxides and Fe, and Al and Si from allophane and allophane-like components. Allophane and imogolite are metastable aluminosilicates that form mainly on easily weathered volcanic glass or other recently deposited volcanic material (e.g., rocks, pumic) [60,94]. Opal and crystalline iron oxides such as hematite or goethite are not dissolved, although this may vary with sample properties [40]. Laboratory procedures followed the instructions of Tamm [38] and Schwertmann [39]. For the ammonium oxalate extraction solution, 28.42 g of $(NH4)2C_2O_4 \times H_2O$ and 18.01 g of the anhydrous oxalic acid ($H_2C_2O_4$) are admixed with 1 L of ultrapure water. For the analysis, 20 reference samples were selected from the stratigraphy, and 0.5 g of dry fine sediment (<2 mm) was mixed with 50 mL of extraction solution, shaken for 2 h in the dark, and then centrifuged. The extract was filtered with qualitative filters, and the determination was carried out in an atomic absorption spectrometer in an Inductively Coupled Plasma Optical Emission Spectrometry (ICP-OES) (Thermo XSeries 2, Accela Pump). The results are given in mg metal/kg of sediment based on the sample weight. The Al_O:Si_O ratio in the AO extract is a commonly used indicator for metastable aluminosilicates such as allophane or imogolite within volcanic soils and sediment [60,94]. According to Churchman and Lowe [6], a linear relationship between oxalate extracted Si and Al, which has been observed in New Zealand soil samples, indicates allophane concentration in the sediment. The availability of Si and Al in the sediment solution is therefore essential to clarify whether allophane, imogolite or halloysite is formed [51,52]. The AO extract thus provides a mea-

sure of both the formation of poorly crystalline oxides as well as of the presence of poorly crystalline aluminosilicates and thus may shed light on diachronic changes in weathering intensities

Appendix B. Results

Table A1. Results of the BC content and the ratio of B5CA/B6CA. For samples labeled "excl.", ratio values are excluded from further interpretation due to the low BC content.

Profile F35							
Sample ID	**Depth (m b.s.)**	**Unit**	**BC (g kg^{-1})**	**STD**	**B5CA/B6CA**	**STD**	
BC1	0.07	I	0.84	0.08	0.95	0.05	
BC2	0.20	II	0.35	0.05	0.77	0.08	
BC3	0.31	III	1.34	0.27	1.03	0.25	
BC4	0.40	III	0.02	0.00	1.36	0.25	excl.
BC5	0.45	III	0.42	0.08	0.89	0.00	
BC6	0.52	IV	0.14	0.04	1.12	0.03	
BC7	0.67	V	0.07	0.00	1.95	1.13	excl.
BC8	0.73	V	1.53	0.44	1.31	0.42	
BC9	0.76	V	0.0033	0.00	1.67	0.00	excl.
BC10	0.93	VI	0.24	0.06	0.79	0.12	
BC11	1.20	VI	0.24	0.03	0.59	0.07	
BC12	1.43	VI	0.23	0.01	0.97	0.10	
BC13	1.62	VII	0.11	0.00	1.28	0.67	
Profile G35							
Sample ID	**Depth (m b.s.)**	**Unit**	**BC (g kg^{-1})**	**STD**	**B5CA/B6CA**	**STD**	
BC14	1.59	VII	0.89	0.08	0.78	0.02	
BC15	1.66	VII	0.97	0.17	0.84	0.08	
BC16	1.77	VII	0.17	0.02	1.78	0.98	excl.
BC17	1.85	VII	0.48	0.08	0,.77	0.11	
BC18	1.92	VII	0.23	0.00	0.76	0.13	
BC19	1.93	VIII	0.21	0.01	0.85	0.08	
BC20	2.00	IX	0.52	0.10	0.79	0.12	

Table A2. Results of the phytolith ratio for both squares F35 and G35. The classification was made according to the three fundamental morphotypes: ELONGATE (ELO), BLOCKY (BLO), ACUTE BULBOSUS (ACU_BUL). Samples that could not be counted correctly are marked with the abbreviation n.c.

Profile F35											
Sample ID	**Depth (m b.s.)**	**Unit**	**BLO light**	**ELO light**	**ACU_BUL light**	**BLO dark**	**ELO dark**	**ACU_BUL dark**	**Sum**	**% light**	**% dark**
SOD_002	0.03	I	30	250	10	9	13	3	315	92.1	7.9
SOD_006	0.13	II	44	146	20	42	52	22	326	64.4	35.6
SOD_009	0.19	III	2	3	1	105	117	104	335	1.8	98.2
SOD_013	0.27	III	26	94	29	91	43	29	312	47.8	52.2
SOD_018	0.37	III	20	108	14	78	68	28	316	44.9	55.1
SOD_025	0.51	IV	5	25	2	124	95	71	322	9.9	90.1
SOD_027	0.55	IV	25	210	13	12	38	13	310	79.7	20.3
SOD_031	0.63	V	3	3	1	133	117	83	340	2.1	97.9
SOD_039	0.79	VI	32	158	23	18	82	37	350	60.9	39.1
SOD_050	1.01	VI	33	121	14	28	106	72	374	44.9	55.1
SOD_060	1.21	VI	15	220	36	11	41	25	348	77.9	22.1
SOD_071	1.43	VI (VII)	44	98	16	38	71	66	333	47.4	52.6
SOD_081	1.63	VII	32	78	14	30	83	67	310	40.3	59.7

Table A2. *Cont.*

Profile G35											
Sample ID	**Depth (m b.s.)**	**Unit**	**BLO light**	**ELO light**	**ACU_BLO light**	**BLO dark**	**ELO dark**	**ACU_BLO dark**	**Sum**	**% light**	**% dark**
SOD_087	1.44	VI (VII)	5	8	3	117	170	113	416	3.8	96.2
SOD_096	1.62	VII	28	138	11	22	84	55	338	52.4	47.6
SOD_103	1.8	VII	20	257	22	9	20	16	344	86.9	13.1
SOD_106	1.86	VII	10	253	18	2	12	9	303	92.7	7.3
SOD_18_03	1.96	VIII	11	223	19	5	32	16	306	82.7	17.3
SOD_18_07	2.04	IX	n.c.	n.c.	n.c.	n.c.	n.c.	n.c.	n.c.	n.c.	n.c.

Table A3. Results of ammonium oxalate extraction showing standard deviation (s) and AlO:SiO ratio. Samples SOD_003 to 083 originate from profile F35 and SOD_86 to SOD_18_07 from profile G35.

Profile F35											
	Depth		Al_O	Al_O s	Fe_O	Fe_O s	Mn_O	Mn_O s	Si_O	Si_O s	
Sample ID	**(m b.s.)**	**Unit**	**(g kg^{-1})**	**(g kg^{-1})**	**(g kg^{-1})**	**(g kg^{-1})**	**(g kg^{-1})**	**(g kg^{-1})**	**(g kg^{-1})**	**(g kg^{-1})**	**Al_O:Si_O**
SOD_003	0.06	I	1.91	0.07	5.97	0.23	1.20	0.19	0.93	0.02	2.06
SOD_007	0.15	II	0.77	0.03	1.84	0.15	0.44	0.00	0.31	0.02	2.47
SOD_009	0.19	III	9.45	0.26	4.98	0.02	1.77	0.01	2.76	0.05	3.42
SOD_015	0.31	III	0.84	0.02	1.87	0.03	0.66	0.01	0.37	0.01	2.26
SOD_018	0.37	III	1.40	0.07	2.98	0.26	1.05	0.11	0.55	0.04	2.53
SOD_025	0.51	IV	0.90	0.12	1.77	0.24	0.92	0.17	0.39	0.06	2.29
SOD_029	0.59	V	7.00	0.39	4.80	0.37	2.77	0.10	2.32	0.28	3.02
SOD_031	0.63	V	17.07	0.45	5.25	0.39	2.23	0.17	5.96	0.42	2.86
SOD_036	0.73	V/VI	1.92	0.03	3.21	0.18	0.51	0.01	0.67	0.03	2.87
SOD_044	0.89	VI	2.07	0.08	7.66	0.16	0.89	0.15	1.02	0.00	2.03
SOD_051	1.03	VI	2.17	0.11	8.15	0.96	0.64	0.09	1.06	0.10	2.06
SOD_054	1.09	VI	2.08	0.05	5.41	0.27	0.68	0.06	0.86	0.05	2.42
SOD_061	1.23	VI	1.98	0.15	6.24	0.76	0.64	0.13	0.91	0.11	2.17
SOD_078	1.57	VII	1.70	0.04	5.26	0.10	0.80	0.09	0.77	0.03	2.20
SOD_083	1.68	VII	2.85	0.11	5.30	0.14	2.26	0.06	1.03	0.04	2.76
Profile G35											
	Depth		Al_o	Al_o s	Fe_o	Fe_o s	Mn_o	Mn_o s	Si_o	Si_o s	
Sample ID	**(m b.s.)**	**Unit**	**(g kg^{-1})**	**(g kg^{-1})**	**(g kg^{-1})**	**(g kg^{-1})**	**(g kg^{-1})**	**(g kg^{-1})**	**(g kg^{-1})**	**(g kg^{-1})**	**Al_O:Si_O**
SOD_086	1.41	VI	2.23	0.11	7.98	0.57	0.80	0.09	1.25	0.09	1.78
SOD_102	1.78	VII	1.39	0.01	3.40	0.11	1.74	0.02	0.59	0.01	2.37
SOD_18_01	1.92	VII	1.47	0.06	3.56	0.30	1.00	0.11	0.56	0.05	2.64
SOD_18_04	1.98	VIII	1.57	0.11	3.77	0.33	1.24	0.15	0.59	0.05	2.68
SOD_18_07	2.04	IX	1.56	0.07	3.96	0.09	1.37	0.03	0.53	0.02	2.96

References

1. Hensel, E.A.; Vogelsang, R.; Noack, T.; Bubenzer, O. Stratigraphy and Chronology of Sodicho Rockshelter–A New Sedimentological Record of Past Environmental Changes and Human Settlement Phases in Southwestern Ethiopia. *Front. Earth Sci.* **2021**, *8*. [CrossRef]
2. Brandt, S.A.; Fisher, E.C.; Hildebrand, E.A.; Vogelsang, R.; Ambrose, S.H.; Lesur, J.; Wang, H. Early MIS 3 occupation of Mochena Borago Rockshelter, Southwest Ethiopian Highlands: Implications for Late Pleistocene archaeology, paleoenvironments and modern human dispersals. *Quat. Int.* **2012**, *274*, 38–54. [CrossRef]
3. Brandt, S.; Hildebrand, E.; Vogelsang, R.; Wolfhagen, J.; Wang, H. A new MIS 3 radiocarbon chronology for Mochena Borago Rockshelter, SW Ethiopia: Implications for the interpretation of Late Pleistocene chronostratigraphy and human behavior. *J. Archaeol. Sci. Rep.* **2017**, *11*, 352–369. [CrossRef]
4. Vogelsang, R.; Wendt, K.P. Reconstructing prehistoric settlement models and land use patterns on Mt. Damota/SW Ethiopia. *Quat. Int.* **2018**, *485*, 140–149. [CrossRef]
5. Waters, M.R. *Principles of Geoarchaeology: A North American Perspective*; University of Arizona Press: Tucson, AZ, USA, 1992; ISBN 0-8165-1770-3.
6. Churchman, G.J.; Lowe, D.J. Alteration, Formation, and Occurrence of Minerals in Soils. In *Handbook of Soil Sciences: Properties and Processes*; CRC Press: Boca Raton, FL, USA, 2012; pp. 1–72.
7. Stoops, G.; Nicosia, C. Introduction. In *Archaeological Soil and Sediment Micromorphology*; Nicosia, C., Stoops, G., Eds.; John Wiley & Sons, Ltd.: Chichester, UK, 2017; pp. 1–5.
8. Mark, B.G.; Osmaston, H.A. Quaternary glaciation in Africa: Key chronologies and climatic implications. *J. Quat. Sci.* **2008**, *23*, 589–608. [CrossRef]
9. Junginger, A.; Trauth, M.H. Hydrological constraints of paleo-Lake Suguta in the Northern Kenya Rift during the African Humid Period (15–5kaBP). *Glob. Planet. Chang.* **2013**, *111*, 174–188. [CrossRef]

10. Stoops, G. *Guidelines for Analysis and Description of Soil and Regolith Thin Sections*; John Wiley & Sons: Hoboken, NJ, USA, 2021; Volume 184.
11. Goldberg, P.; Miller, C.E.; Schiegl, S.; Ligouis, B.; Berna, F.; Conard, N.J.; Wadley, L. Bedding, hearths, and site maintenance in the Middle Stone Age of Sibudu Cave, KwaZulu-Natal, South Africa. *Archaeol. Anthropol. Sci.* **2009**, *1*, 95–122. [CrossRef]
12. Marean, C.W.; Bar-Matthews, M.; Fisher, E.; Goldberg, P.; Herries, A.; Karkanas, P.; Nilssen, P.J.; Thompson, E. The stratigraphy of the Middle Stone Age sediments at Pinnacle Point Cave 13B (Mossel Bay, Western Cape Province, South Africa). *J. Hum. Evol.* **2010**, *59*, 234–255. [CrossRef]
13. Miller, C.E.; Goldberg, P.; Berna, F. Geoarchaeological investigations at Diepkloof Rock Shelter, Western Cape, South Africa. *J. Archaeol. Sci.* **2013**, *40*, 3432–3452. [CrossRef]
14. Inglis, R.H.; French, C.; Farr, L.; Hunt, C.O.; Jones, S.; Reynolds, T.; Barker, G. Sediment micromorphology and site formation processes during the Middle to Later Stone Ages at the Haua Fteah Cave, Cyrenaica, Libya. *Geoarchaeology* **2017**, *33*, 328–348. [CrossRef]
15. Klasen, N.; Kehl, M.; Mikdad, A.; Brückner, H.; Weniger, G.-C. Chronology and formation processes of the Middle to Upper Palaeolithic deposits of Ifri n'Ammar using multi-method luminescence dating and micromorphology. *Quat. Int.* **2018**, *485*, 89–102. [CrossRef]
16. Potì, A.; Kehl, M.; Broich, M.; Marco, Y.C.; Hutterer, R.; Jentke, T.; Linstädter, J.; López-Sáez, J.A.; Mikdad, A.; Morales, J.; et al. Human occupation and environmental change in the western Maghreb during the Last Glacial Maximum (LGM) and the Late Glacial. New evidence from the Iberomaurusian site Ifri El Baroud (northeast Morocco). *Quat. Sci. Rev.* **2019**, *220*, 87–110. [CrossRef]
17. Goldberg, P.; Bar-Yosef, O. Site Formation Processes in Kebara and Hayonim Caves and Their Significance in Levantine Prehistoric Caves. In *Neandertals and Modern Humans in Western Asia*; Akazawa, T., Aoki, K., Bar-Yosef, O., Eds.; Springer: Boston, MA, USA, 2005; pp. 107–125.
18. Albert, R.M.; Berna, F.; Goldberg, P. Insights on Neanderthal fire use at Kebara Cave (Israel) through high resolution study of prehistoric combustion features: Evidence from phytoliths and thin sections. *Quat. Int.* **2012**, *247*, 278–293. [CrossRef]
19. Kehl, M.; Burow, C.; Cantalejo, P.; Domínguez-Bella, S.; Durán, J.J.; Henselowsky, F.; Klasen, N.; Linstädter, J.; Medianero, J.; Pastoors, A.; et al. Site formation and chronology of the New Paleolithic Site Sima de Las Palomas de Teba, Southern Spain. *Quat. Res.* **2016**, *85*, 313–331. [CrossRef]
20. Miller, C.E. *A Tale of Two Swabian Caves: Geoarchaeological Investigations at Hohle Fels and Geißenklösterle*; Kerns Verlag: Tübingen, Germany, 2015; ISBN 3-935751-19-2.
21. Whitau, R.; Vannieuwenhuyse, D.; Dotte-Sarout, E.; Balme, J.; O'Connor, S. Home Is Where the Hearth Is: Anthracological and Microstratigraphic Analyses of Pleistocene and Holocene Combustion Features, Riwi Cave (Kimberley, Western Australia). *J. Archaeol. Method Theory* **2018**, *25*, 739–776. [CrossRef] [PubMed]
22. Brancaleoni, G.; Shnaider, S.; Osipova, E.; Danukalova, G.; Kurbanov, R.; Deput, E.; Kyzy, S.A.; Abdykanova, A.; Krajcarz, M.T. Depositional history of a talus cone in an arid intermontane basin in Central Asia: An interdisciplinary study at the Late Pleistocene–Late Holocene Obishir-I site, Kyrgyzstan. *Geoarchaeology* **2021**, 1–24. [CrossRef]
23. Morley, M.W.; Goldberg, P.; Uliyanov, V.A.; Kozlikin, M.B.; Shunkov, M.V.; Derevianko, A.P.; Jacobs, Z.; Roberts, R.G. Hominin and animal activities in the microstratigraphic record from Denisova Cave (Altai Mountains, Russia). *Sci. Rep.* **2019**, *9*, 13785. [CrossRef] [PubMed]
24. Kolobova, K.A.; Roberts, R.G.; Chabai, V.P.; Jacobs, Z.; Krajcarz, M.T.; Shalagina, A.V.; Krivoshapkin, A.I.; Li, B.; Uthmeier, T.; Markin, S.V.; et al. Archaeological evidence for two separate dispersals of Neanderthals into southern Siberia. *Proc. Natl. Acad. Sci. USA* **2020**, *117*, 2879–2885. [CrossRef] [PubMed]
25. Goldberg, E.D. *Black Carbon in the Environment: Properties and Distribution*; John Wiley and Sons: New York, NY, USA, 1985.
26. Schmidt, M.W.I.; Noack, A.G. Black carbon in soils and sediments: Analysis, distribution, implications, and current challenges. *Glob. Biogeochem. Cycles* **2000**, *14*, 777–793. [CrossRef]
27. Keiluweit, M.; Nico, P.S.; Johnson, M.G.; Kleber, M. Dynamic Molecular Structure of Plant Biomass-Derived Black Carbon (Biochar). *Environ. Sci. Technol.* **2010**, *44*, 1247–1253. [CrossRef]
28. Masiello, C.A.; Druffel, E.R.M. Black Carbon in Deep-Sea Sediments. *Science* **1998**, *280*, 1911–1913. [CrossRef] [PubMed]
29. Scott, A.C.; Glasspool, I.J. The diversification of Paleozoic fire systems and fluctuations in atmospheric oxygen concentration. *Proc. Natl. Acad. Sci. USA* **2006**, *103*, 10861–10865. [CrossRef] [PubMed]
30. Wolf, M.; Lehndorff, E.; Mrowald, M.; Eckmeier, E.; Kehl, M.; Frechen, M.; Pätzold, S.; Amelung, W. Black carbon: Fire fingerprints in Pleistocene loess–palaeosol archives in Germany. *Org. Geochem.* **2014**, *70*, 44–52. [CrossRef]
31. Brodowski, S.; Rodionov, A.; Haumaier, L.; Glaser, B.; Amelung, W. Revised black carbon assessment using benzene polycarboxylic acids. *Org. Geochem.* **2005**, *36*, 1299–1310. [CrossRef]
32. Glaser, B.; Haumaier, L.; Guggenberger, G.; Zech, W. Black carbon in soils: The use of benzenecarboxylic acids as specific markers. *Org. Geochem.* **1998**, *29*, 811–819. [CrossRef]
33. Wolf, M.; Lehndorff, E.; Wiesenberg, G.; Stockhausen, M.; Schwark, L.; Amelung, W. Towards reconstruction of past fire regimes from geochemical analysis of charcoal. *Org. Geochem.* **2013**, *55*, 11–21. [CrossRef]
34. Vrydaghs, L.; Devos, Y.; Pető, Á. Opal Phytoliths. In *Archaeological Soil and Sediment Micromorphology*; John Wiley & Sons, Ltd.: Chichester, UK, 2017; pp. 155–163.

35. Kaczorek, D.; Vrydaghs, L.; Devos, Y.; Pető, Á.; Effland, W.R. Biogenic Siliceous Features. In *Interpretation of Micromorphological Features of Soils and Regoliths*, 2nd ed.; Stoops, G., Marcelino, V., Mees, F., Eds.; Elsevier: Amsterdam, The Netherlands; Oxford, UK, 2018; pp. 157–176, ISBN 978-0-444-63522-8.
36. Neumann, K.; Strömberg, C.A.E.; Ball, T.; Albert, R.M.; Vrydaghs, L.; Cummings, L.S. International Code for Phytolith Nomenclature (ICPN) 2.0. *Ann. Bot.* **2019**, *124*, 189–199. [CrossRef]
37. Parr, J.F. Effect of fire on phytolith coloration. *Geoarchaeology* **2006**, *21*, 171–185. [CrossRef]
38. Tamm, O. Über ie Oxalatmethode in der chemischen Bodenanalyse. *Med. Följer Skogsvärdsföreningens Tidskr.* **1932**, *27*, 1–20.
39. Schwertmann, U. Der einfluss einfacher organischer anionen auf die bildung von goethit und hämatit aus amorphen Fe(III)-Hydroxid. *Geoderma* **1970**, *3*, 207–214. [CrossRef]
40. Rennert, T. Wet-chemical extractions to characterise pedogenic Al and Fe species–A critical review. *Soil Res.* **2019**, *57*, 1–16. [CrossRef]
41. Woldegabriel, G.; Aronson, J.L.; Walter, R. Geology, geochronology, and rift basin development in the central sector of the Main Ethiopia Rift. *GSA Bull.* **1990**, *102*, 439–458. [CrossRef]
42. WoldeGabriel, G.; Walter, R.C.; Aronson, J.L.; Hart, W.K. Geochronology and distribution of silicic volcanic rocks of Plio-Pleistocene age from the central sector of the Main Ethiopian Rift. *Quat. Int.* **1992**, *13–14*, 69–76. [CrossRef]
43. Chernet, T. Geology and hydrothermal resources in the northern Lake Abaya area (Ethiopia). *J. Afr. Earth Sci.* **2011**, *61*, 129–141. [CrossRef]
44. Hensel, E.A.; Bödeker, O.; Bubenzer, O.; Vogelsang, R. Combining geomorphological–hydrological analyses and the location of settlement and raw material sites–A case study on understanding prehistoric human settlement activity in the southwestern Ethiopian Highlands. *E&G Quat. Sci. J.* **2019**, *68*, 201–213. [CrossRef]
45. Berhanu, B.; Melesse, A.M.; Seleshi, Y. GIS-based hydrological zones and soil geo-database of Ethiopia. *Catena* **2013**, *104*, 21–31. [CrossRef]
46. IUSS Working Group WRB. *World Reference Base for Soil Resources 2014: International Soil Classification System for Naming Soils and Creating Legends for Soil Maps*; FAO: Rome, Italy, 2015; Volume 106.
47. Gutherz, X.; Jallot, L.; Lesur, J.; Pouzolles, G.; Sordoillet, D. Les fouilles de l'abri sous-roche de Moche Borago (Soddo-Wolayta). Premier bilan. *Ann. D'ethiopie* **2002**, *18*, 181–190. [CrossRef]
48. Fisher, E.C. Late Pleistocene Technological Change and Hunter Gatherer Behavior at Moche Borago Rockshelter, Sodo-Wolayta, Ethiopia: Flaked Stone Artifacts from the Early OIS 3 (60–43 Ka) Deposits. Ph.D. Thesis, University of Florida, Gainesville, FL, USA, 2010.
49. Mentzer, S.M. Microarchaeological Approaches to the Identification and Interpretation of Combustion Features in Prehistoric Archaeological Sites. *J. Archaeol. Method Theory* **2014**, *21*, 616–668. [CrossRef]
50. Stoops, G.; Sedov, S.; Shoba, S. Regoliths and Soils on Volcanic Ash. In *Interpretation of Micromorphological Features of Soils and Regoliths*, 2nd ed.; Elsevier: Amsterdam, The Netherlands; Oxford, UK, 2018; pp. 721–751.
51. Parfitt, R.L.; Furkert, R.J.; Henmi, T. Identification and Structure of Two Types of Allophane from Volcanic Ash Soils and Tephra. *Clays Clay Miner.* **1980**, *28*, 328–334. [CrossRef]
52. Farmer, V.C.; McHardy, W.J.; Robertson, L.; Walker, A.; Wilson, M.J. Micromorphology and sub-microscopy of allophane and imogolite in a podzol Bs horizon: Evidence for translocation and origin. *J. Soil Sci.* **1985**, *36*, 87–95. [CrossRef]
53. Churchman, G.J.; Velde, B. *Soil Clays: Linking Geology, Biology, Agriculture, and the Environment*; CRC Press: Boca Raton, FL, USA, 2019; ISBN 0-429-53224-5.
54. Gillhuber, S.; Lehrberger, G.; Thuro, K. Teplá Trachyte Weathering Phenomena and Physical Properties of a Rare Volcanogenic Building Stone. *Geol. Soc. Lond.* **2006**, *469*, 1–11.
55. Foerster, V.; Junginger, A.; Langkamp, O.; Gebru, T.; Asrat, A.; Umer, M.; Lamb, H.F.; Wennrich, V.; Rethemeyer, J.; Nowaczyk, N.; et al. Climatic change recorded in the sediments of the Chew Bahir basin, southern Ethiopia, during the last 45,000 years. *Quat. Int.* **2012**, *274*, 25–37. [CrossRef]
56. Foerster, V.; Vogelsang, R.; Junginger, A.; Asrat, A.; Lamb, H.; Schaebitz, F.; Trauth, M. Environmental change and human occupation of southern Ethiopia and northern Kenya during the last 20,000 years. *Quat. Sci. Rev.* **2015**, *129*, 333–340. [CrossRef]
57. Hildebrand, E.A.; Brandt, S.A.; Friis, I.; Demissew, S. Paleoenvironmental Reconstructions for the Horn of Africa: Interdisciplinary Perspectives on Strategy and Significance. In *Trees, Grasses and Crops. People and Plants in Sub-saharan Africa and Beyond*; Verlag Dr. Rudolf Habelt: Bonn, Germany, 2019; pp. 187–210, ISBN 3-7749-4221-8.
58. Trauth, M.H.; Asrat, A.; Duesing, W.; Foerster, V.; Kraemer, K.H.; Marwan, N.; Maslin, M.; Schaebitz, F. Classifying past climate change in the Chew Bahir basin, southern Ethiopia, using recurrence quantification analysis. *Clim. Dyn.* **2019**, *53*, 2557–2572. [CrossRef]
59. Chadwick, O.A.; Gavenda, R.T.; Kelly, E.F.; Ziegler, K.; Olson, C.G.; Elliott, W.; Hendricks, D.M. The impact of climate on the biogeochemical functioning of volcanic soils. *Chem. Geol.* **2003**, *202*, 195–223. [CrossRef]
60. Parfitt, R.; Henmi, T. Comparison of an oxalate-extraction methon and an infrared spectroscopic method for determining allophane in soll clays. *Soil Sci. Plant Nutr.* **1982**, *28*, 183–190. [CrossRef]
61. Stoops, G.; Marcelino, V. Lateritic and Bauxitic Materials. In *Interpretation of Micromorphological Features of Soils and Regoliths*, 2nd ed.; Stoops, G., Marcelino, V., Mees, F., Eds.; Elsevier: Amsterdam, The Netherlands; Oxford, UK, 2018; pp. 691–720.

62. Kühn, P.; Aguilar, J.; Miedema, R.; Bronnikova, M. Textural Pedofeatures and Related Horizons. In *Interpretation of Micromorphological Features of Soils and Regoliths*, 2nd ed.; Stoops, G., Marcelino, V., Mees, F., Eds.; Elsevier: Amsterdam, The Netherlands; Oxford, UK, 2018; pp. 377–423, ISBN 978-0-444-63522-8.
63. Karkanas, P. Chemical Alteration. In *Encyclopedia of Geoarchaeology*; Gilbert, A.S., Ed.; Springer: Dordrecht, The Netherlands, 2017; pp. 129–138, ISBN 978-1-4020-4409-0.
64. Stoops, G.; Mees, F. Groundmass Composition and Fabric. In *Interpretation of Micromorphological Features of Soils and Regoliths*, 2nd ed.; Stoops, G., Marcelino, V., Mees, F., Eds.; Elsevier: Amsterdam, The Netherlands; Oxford, UK, 2018; pp. 73–125.
65. Vepraskas, M.J.; Lindbo, D.L.; Stolt, M.H. Redoximorphic Features. In *Interpretation of Micromorphological Features of Soils and Regoliths*, 2nd ed.; Stoops, G., Marcelino, V., Mees, F., Eds.; Elsevier: Amsterdam, The Netherlands; Oxford, UK, 2018; pp. 425–445, ISBN 978-0-444-63522-8.
66. Goldberg, P.; Berna, F.; Chazan, M. Deposition and Diagenesis in the Earlier Stone Age of Wonderwerk Cave, Excavation 1, South Africa. *Afr. Archaeol. Rev.* **2015**, *32*, 613–643. [CrossRef]
67. Villagran, X.S.; Balbo, A.L.; Madella, M.; Vila, A.; Estevez, J. Experimental micromorphology in Tierra del Fuego (Argentina): Building a reference collection for the study of shell middens in cold climates. *J. Archaeol. Sci.* **2011**, *38*, 588–604. [CrossRef]
68. Mallol, C.; Mentzer, S.M.; Miller, C.E. Combustion Features. In *Archaeological Soil and Sediment Micromorphology*; John Wiley & Sons, Ltd.: Chichester, UK, 2017; pp. 299–330.
69. Fischer, M.L.; Bachofer, F.; Yost, C.L.; Bludau, I.J.E.; Schepers, C.; Foerster, V.; Lamb, H.; Schäbitz, F.; Asrat, A.; Trauth, M.H.; et al. A Phytolith Supported Biosphere-Hydrosphere Predictive Model for Southern Ethiopia: Insights into Paleoenvironmental Changes and Human Landscape Preferences since the Last Glacial Maximum. *Geosciences* **2021**, *11*, 418. [CrossRef]
70. Kooistra, M.J.; Pulleman, M.M. Features Related to Faunal Activity. In *Interpretation of Micromorphological Features of Soils and Regoliths*, 2nd ed.; Stoops, G., Marcelino, V., Mees, F., Eds.; Elsevier: Amsterdam, The Netherlands; Oxford, UK, 2018; pp. 447–469, ISBN 978-0-444-63522-8.
71. Parfitt, R.L. Allophane and imogolite: Role in soil biogeochemical processes. *Clay Miner.* **2009**, *44*, 135–155. [CrossRef]
72. Goldberg, P.; Holliday, V.T.; Ferring, C.R. *Earth Sciences and Archaeology*; Kluwer Academic/Plenum Publishers: New York, NY, USA, 2001; ISBN 978-0-306-46279-5.
73. Tarasenko, I.; Bielders, C.L.; Guevara, A.; Delmelle, P. Surface crusting of volcanic ash deposits under simulated rainfall. *Bull. Volcanol.* **2019**, *81*, 30. [CrossRef]
74. Williams, G.T.; Jenkins, S.F.; Lee, D.W.J.; Wee, S.J. How rainfall influences tephra fall loading—An experimental approach. *Bull. Volcanol.* **2021**, *83*, 42. [CrossRef]
75. Goldberg, P.; Aldeias, V. Why does (archaeological) micromorphology have such little traction in (geo)archaeology? *Archaeol. Anthr. Sci.* **2018**, *10*, 269–278. [CrossRef]
76. Karkanas, P.; Goldberg, P. Phosphatic Features. In *Interpretation of Micromorphological Features of Soils and Regoliths*, 2nd ed.; Stoops, G., Marcelino, V., Mees, F., Eds.; Elsevier: Amsterdam, The Netherlands; Oxford, UK, 2018; pp. 323–346, ISBN 978-0-444-63522-8.
77. Lambrecht, G.; de Vera, C.R.; Jambrina-Enríquez, M.; Crevecoeur, I.; Gonzalez-Urquijo, J.; Lazuen, T.; Monnier, G.; Pajović, G.; Tostevin, G.; Mallol, C. Characterisation of charred organic matter in micromorphological thin sections by means of Raman spectroscopy. *Archaeol. Anthr. Sci.* **2021**, *13*, 13. [CrossRef] [PubMed]
78. Homsey, L.K.; Capo, R.C. Integrating geochemistry and micromorphology to interpret feature use at Dust Cave, a Paleo-Indian through middle-archaic site in Northwest Alabama. *Geoarchaeology* **2006**, *21*, 237–269. [CrossRef]
79. Canti, M.; Linford, N. The Effects of Fire on Archaeological Soils and Sediments: Temperature and Colour Relationships. *Proc. Prehist. Soc.* **2000**, *66*, 385–395. [CrossRef]
80. Röpke, A.; Dietl, C. Burnt Soils and Sediments. In *Archaeological Soil and Sediment Micromorphology*; John Wiley & Sons, Ltd.: Chichester, UK, 2017; pp. 173–180.
81. Rodríguez-Rodríguez, A.; Fedoroff, N.; Tejedor-Salguero, M.L.; Fernández-Caldas, E. Observaciones Preliminares Sobre La Alteración En Los Suelos Fersialíticos Sobre Materiales Volcánicos (Islas Canarias). *An. Edafol. Agrobiol.* **1980**, *39*, 1923–1939.
82. Goldberg, P. Micromorphology of Pech-de-l'Azé II sediments. *J. Archaeol. Sci.* **1979**, *6*, 17–47. [CrossRef]
83. Goldberg, P. Some Observations on Middle and Upper Palaeolithic Ashy Cave and Rockshelter Deposits in the Near East. In *More than Meets the Eye: Studies on Upper Palaeolithic Diversity in the Near East*; Oxbow Books: Oxford, UK, 2003; pp. 19–32.
84. Dibble, H.; Berna, F.; Goldberg, P.; McPherron, S.; Mentzer, S.; Niven, L.; Richter, D.; Sandgathe, D.; Théry-Parisot, I.; Turq, A. A Preliminary Report on Pech de l'Azé IV, Layer 8 (Middle Paleolithic, France). *PaleoAnthropology* **2009**, *2009*, 182–219. [CrossRef]
85. Schneider, M.P.; Hilf, M.; Vogt, U.F.; Schmidt, M.W. The benzene polycarboxylic acid (BPCA) pattern of wood pyrolyzed between 200 °C and 1000 °C. *Org. Geochem.* **2010**, *41*, 1082–1088. [CrossRef]
86. Lehndorff, E.; Linstädter, J.; Kehl, M.; Weniger, G.-C. Fire history reconstruction from Black Carbon analysis in Holocene cave sediments at Ifri Oudadane, Northeastern Morocco. *Holocene* **2015**, *25*, 398–402. [CrossRef]
87. Braadbaart, F.; Poole, I. Morphological, chemical and physical changes during charcoalification of wood and its relevance to archaeological contexts. *J. Archaeol. Sci.* **2008**, *35*, 2434–2445. [CrossRef]
88. Piperno, D.R. *Phytoliths: A Comprehensive Guide for Archaeologists and Paleoecologists*; AltaMira Press: Lanham, MD, USA, 2006; ISBN 0-7591-1446-3.
89. Beckmann, T. Präparation Bodenkundlicher Dünnschliffe Für Mikromorphologische Untersuchungen. *Hohenh. Bodenkd. Hefte* **1997**, *40*, 86–103.

90. Arpin, T.L.; Mallol, C.; Goldberg, P. Short contribution: A new method of analyzing and documenting micromorphological thin sections using flatbed scanners: Applications in geoarchaeological studies. *Geoarchaeology* **2002**, *17*, 305–313. [CrossRef]
91. Mörchen, R.; Lehndorff, E.; Diaz, F.A.; Moradi, G.; Bol, R.; Fuentes, B.; Klumpp, E.; Amelung, W. Carbon accrual in the Atacama Desert. *Glob. Planet. Chang.* **2019**, *181*, 102993. [CrossRef]
92. Kappenberg, A.; Bläsing, M.; Lehndorff, E.; Amelung, W. Black carbon assessment using benzene polycarboxylic acids: Limitations for organic-rich matrices. *Org. Geochem.* **2016**, *94*, 47–51. [CrossRef]
93. Hammes, K.; Schmidt, M.W.I.; Smernik, R.J.; Currie, L.A.; Ball, W.P.; Nguyen, T.H.; Louchouarn, P.; Houel, S.; Gustafsson, Ö.; Elmquist, M.; et al. Comparison of quantification methods to measure fire-derived (black/elemental) carbon in soils and sediments using reference materials from soil, water, sediment and the atmosphere. *Glob. Biogeochem. Cycles* **2007**, *21*, GB3016. [CrossRef]
94. Harsh, J.; Chorover, J.; Nizeyimana, E. Allophane and Imogolite. In *Soil Mineralogy with Environmental Applications*; Soil Science Society of America: Madison, WI, USA, 2002; Volume 7, pp. 291–322.